Heliyon 10 (2024) e32154

Contents lists available at ScienceDirect

Heliyon

journal homepage: www.cell.com/heliyon

Research article

Immunotherapy-relevance of a candidate prognostic score for Acute Myeloid Leukemia

Yiyun Pan [a,b,1], Wen Zeng [b,1], Xiaoming Nie [b,1], Hailong Chen [b], Chuanhua Xie [b], Shouju Guo [b], Dechang Xu [b,**], Yijian Chen [a,c,*]

[a] Suzhou Medical College of Soochow University, Suzhou, 215123, Jiangsu, China
[b] Ganzhou Cancer Hospital, Gannan Medical University, Ganzhou, 341000, Jiangxi, China
[c] The First Affiliated Hospital of Gannan Medical University, Ganzhou, 341000, Jiangxi, China

ARTICLE INFO

Keywords:
Acute myeloid leukemia
Cancer immunotherapy
Prognostic score
Transcriptome

ABSTRACT

Background: Acute Myeloid Leukemia (AML) exhibits a wide array of phenotypic manifestations, progression patterns, and heterogeneous responses to immunotherapies, suggesting involvement of complex immunobiological mechanisms. This investigation aimed to develop an integrated prognostic model for AML by incorporating cancer driver genes, along with clinical and phenotypic characteristics of the disease, and to assess its implications for immunotherapy responsiveness.

Methods: Critical oncogenic driver genes linked to survival were identified by screening primary effector and corresponding gene pairs using data from The Cancer Genome Atlas (TCGA), through univariate Cox proportional hazard regression analysis. This was independently verified using dataset GSE37642. Primary effector genes were further refined using LASSO regression. Transcriptomic profiling was quantified using multivariate Cox regression, and the derived prognostic score was subsequently validated. Finally, a multivariate Cox regression model was developed, incorporating the transcriptomic score along with clinical parameters such as age, gender, and French-American-British (FAB) classification subtype. The 'Accurate Prediction Model of AML Overall Survival Score' (APMAO) was developed and subsequently validated. Investigations were conducted into functional pathway enrichment, alterations in the gene mutational landscape, and the extent of immune cell infiltration associated with varying APMAO scores. To further investigate the potential of APMAO scores as a predictive biomarker for responsiveness to cancer immunotherapy, we conducted a series of analyses. These included examining the expression profiles of genes related to immune checkpoints, the interferon-gamma signaling pathway, and m6A regulation. Additionally, we explored the relationship between these gene expression patterns and the Tumor Immune Dysfunction and Exclusion (TIDE) dysfunction scores.

Results: Through the screening of 95 cancer genes associated with survival and 313 interacting gene pairs, seven genes (ACSL6, MAP3K1, CHIC2, HIP1, PTPN6, TFEB, and DAXX) were identified, leading to the derivation of a transcriptional score. Age and the transcriptional score were significant predictors in Cox regression analysis and were integral to the development of the final

* Corresponding author. The First Affiliated Hospital of Gannan Medical University. No.23, Qingnian Road, Zhanggong Avenue, Ganzhou, Jiangxi, China.
** Corresponding author.
E-mail addresses: 947271147@qq.com (Y. Pan), 657636369@qq.com (W. Zeng), 839906364@qq.com (X. Nie), chl2588896@163.com (H. Chen), 737468682@qq.com (C. Xie), jxgzguosj@126.com (S. Guo), gzwyxdc@126.com (D. Xu), chenyj2005@gmu.edu.cn (Y. Chen).
[1] Contributed equally.

https://doi.org/10.1016/j.heliyon.2024.e32154
Received 26 July 2023; Received in revised form 28 May 2024; Accepted 29 May 2024
Available online 29 May 2024

APMAO model, which exhibited an AUC greater than 0.75 and was successfully validated. Notable differences were observed in the distribution of the transcriptional score, age, cytogenetic risk categories, and French-American-British (FAB) classification between high and low APMAO groups. Samples with high APMAO scores demonstrated significantly higher mutation rates and pathway enrichments in NFKB, TNF, JAK-STAT, and NOTCH signaling. Additionally, variations in immune cell infiltration and immune checkpoint expression, activation of the interferon-γ pathway, and expression of m6A regulators were noted, including a negative correlation between CD160, m6A expression, and APMAO scores.

Conclusion: The combined APMAO score integrating transcriptional and clinical parameters demonstrated robust prognostic performance in predicting AML survival outcomes. It was linked to unique phenotypic characteristics, distinctive immune and mutational profiles, and patterns of expression for markers related to immunotherapy sensitivity. These observations suggest the potential for facilitating precision immunotherapy and advocate for its exploration in upcoming clinical trials.

1. Introduction

Acute myeloid leukemia (AML) represents a diverse collection of hematologic cancers that originate in the bone marrow and are characterized by the clonal expansion of precursor cells of the myeloid lineage [1]. AML incidence rises substantially with increasing age, with a reported median age at diagnosis ranging from 65 to 71 years, making it the most prevalent hematologic malignancy [2,3]. Over the past three decades, the global burden of AML has surged by 87.3 %, with Western Europe and South Asia experiencing the most notable escalation in disease prevalence. Factors such as smoking, obesity, and chemical exposure have emerged as significant contributors to AML-related mortality [4]. Given the aging demographic profile worldwide and the consequent surge in disease prevalence, effective treatment strategies for AML have become increasingly crucial. Genetic aberrations are central to the pathogenesis of acute myeloid leukemia (AML) and constitute a major focus of current research. Particular attention is given to epigenetic

Table 1
Clinical and molecular characteristics of the TCGA-LAML cohort. The table summarizes the distribution of age, gender, French-American-British (FAB) classification subtypes, cytogenetic risk categories, and mutation status of FLT3, NPM1, and RUNX1 genes among the patients in the dataset.

	TCGA-LAML
Age (years)	
>65	34
≤65	98
Gender	
Male	71
Female	61
FAB	
M0 Undifferentiated	12
M1	32
M2	32
M3	14
M4	27
M5	12
M6	2
M7	1
cytogenetic_risk_category	
Favorable	30
Intermediate/Normal	73
Poor	27
NA	2
FLT3-Mut	
Wt	51
Mut	2
NA	79
NPM1-Mut	
Wt	48
Mut	5
NA	79
RUNX1-Mut	
Wt	47
Mut	6
NA	79

regulators like DNMT3A, TET2, and ASXL1, which are implicated in the clonal expansion of hematopoietic cells in the aging population [5]. Advancements in our understanding of the genetic landscape of AML have led to refinements in disease classification and therapeutic approaches [6,7].

Acute myeloid leukemia (AML) is a diagnostic umbrella term that captures a spectrum of heterogeneous clinical characteristics, prognostic outcomes, and variabilities in treatment response [8]. The tumor heterogeneity observed in AML manifests as diverse variations in immunophenotype, cytogenetic profiles, and molecular characteristics, presenting challenges in the accurate detection of residual disease and the prediction of relapse [9]. Understanding the intricate interplay between genetic and phenotypic diversity in AML remains a focal point of ongoing research endeavors, aiming to advance precision medicine strategies that enhance treatment efficacy through the tailored utilization of immunotherapy, chemotherapeutic agents, and other targeted therapies [10]. Furthermore, current knowledge regarding the molecular determinants of drug resistance in residual and recurrent acute myeloid leukemia (AML) remains incomplete. Relapse, driven by the refractory nature of recurrent disease, continues to be the predominant cause of mortality associated with AML [11]. Prior research has delineated transcriptional profiles and gene clusters capable of forecasting relapse risk within distinct clinical subgroups of acute myeloid leukemia (AML) [12]. Moreover, machine learning techniques and associated algorithms have been employed to discern transcriptomic characteristics predictive of disease progression and survival outcomes in AML [13–16]. Some AML prognostic scoring models have incorporated immune cell features and composition data, as well as integrated clinical and molecular features to develop improved risk scoring systems [17,18]. In clinical practice, acute myeloid leukemia (AML) risk stratification has predominantly relied on cytogenetic findings, posing challenges as more than half of AML cases exhibit a cytogenetically normal profile [19]. A recent investigation has confirmed the effectiveness of a comprehensive model for risk stratification and prognosis in acute myeloid leukemia (AML), integrating both clinical and molecular features [20]. In this research, our objective was to develop and validate an extensive prognostic scoring system, termed "Accurate Prediction Model of AML Overall Survival Score" (APMAO). This model was constructed by amalgamating data on the expression of cancer driver genes with tumor phenotypic information. Additionally, we explored the functional pathways, mutational profiles, immune cell distributions, and markers of responsiveness to immunotherapy correlated with the APMAO score.

2. Materials and methods

2.1. Data collection

To investigate the key oncogenic drivers associated with prognosis in acute myeloid leukemia (AML), we integrated data from multiple public databases. Gene expression, clinical phenotype, and survival information from the TCGA-LAML cohort were extracted using the R package TCGAmutations (v0.3.0) (Table 1). As a validation cohort, the GSE37642 dataset, containing data from 562 AML patients, was downloaded from the GEO database (Table 2) [21–24]. To accurately annotate human genes, we obtained the gene annotation file in gtf format from the Ensembl database [25]. Furthermore, we referred to previously published pan-cancer immune metagene data [26], and somatic mutation information of cancer-related genes recorded in the COSMIC database (https://cancer.sanger.ac.uk/census#) [27] for subsequent analyses.

RNA-seq data (level 3 FPKM values) for the TCGA-LAML cohort were obtained directly from the TCGA database. These data had

Table 2
Clinical and molecular characteristics of the GSE37642 cohort. The table presents the distribution of age, French-American-British (FAB) classification subtypes, and RUNX1 mutation status among the patients in the dataset. Data on certain variables are not available (NA) for some patients.

	GSE37642
Age (years)	
>65	37
≤65	99
FAB	
0	8
1	29
2	47
3	7
4	17
5	19
6	7
7	1
NA	1
RUNX1-Mut	
Wt	16
Mut	108
NA	12

already undergone quality control, normalization, and log2 transformation by the TCGA consortium. For the GSE37642 dataset, which was generated using microarray technology, we directly obtained the normalized gene expression data from the GEO database.The GEO database provides preprocessed and normalized data that have been subjected to standard normalization methods by the original authors.

2.1.1. Identification of cancer driver genes

To identify potential cancer driver genes associated with overall survival (OS), we performed univariate Cox proportional hazard regression analysis using the R packages survivor (version 3.2–7) and survminer (version 0.4.8). Genes with p-values less than 0.05 were considered significantly correlated with OS and were selected for further validation. The prognostic significance of these candidate cancer driver genes was then independently assessed in the GSE37642 dataset. Genes that exhibited consistent associations with survival outcomes ($p < 0.05$) in both the TCGA and GSE37642 cohorts were designated as primary effector cancer driver genes for subsequent analyses.

To identify strongly interacting gene pairs among the cancer driver genes in the TCGA dataset, we conducted Pearson correlation analysis. Gene pairs exhibiting significant correlations, defined as having an absolute correlation coefficient (|cor|) greater than 0.6 and an adjusted p-value below 0.05, were selected for further investigation.These identified gene pairs were then subject to validation within the GSE37642 dataset using identical criteria. Gene pairs that consistently demonstrated high correlation across both the TCGA and GSE37642 datasets were acknowledged as interacting gene pairs for further investigative analysis.

The primary effector cancer driver genes identified in the previous step were combined with the interacting gene pairs to form a comprehensive gene set. Given the high dimensionality of this gene set, we employed the least absolute shrinkage and selection operator (LASSO) regression method to reduce the number of genes, using the 'glmnet' package (version 4.0–2) in R. To identify genes significantly associated with survival for subsequent modeling, we performed both univariate and multivariate Cox proportional hazard regression analyses using the 'survival' package. The prognostic significance of the primary effector genes was visualized by generating Kaplan-Meier (KM) survival curves with the 'survminer' package, and log-rank tests were used to evaluate differences in survival between groups. Furthermore, the relationships between interacting gene pairs were visually represented using correlation scatter plots.

Development and Validation of the Accurate Prediction Model of AML Overall Survival (APMAO) Score: Integration of Clinical Features and Transcriptomic Data.

Transcriptome scores were initially derived by performing multivariate Cox regression analysis, considering genes with p-values less than 0.05 as significantly associated with survival.Transcriptome scores were then computed according to the specified equation 〖Transcriptional_Score〗 _i = ∑_(j = 1)^;n▒exp_ji- 〖 × β_j 〗 ,where exp represents the expression level of the gene in question, β signifies the regression coefficient derived from multivariate Cox regression for each gene. The Transcriptional_Score for each sample was obtained by summing the products of the expression levels and their corresponding regression coefficients across all significant genes. To evaluate the prognostic value of the Transcriptional_Score, TCGA samples were divided into high and low score groups using the median score as the cutoff. Kaplan-Meier (KM) survival curves were generated for the high and low score groups, and overall survival (OS) data were used to calculate p-values. A p-value <0.05 was considered statistically significant, indicating a meaningful difference in survival between the high and low Transcriptional_Score groups.

Next, we performed a multivariate Cox regression analysis to predict overall survival (OS) by integrating the Transcriptional_Score with clinical variables such as age, gender, and French-American-British (FAB) classification of AML. Variables with p-values <0.05 were considered significantly associated with survival outcomes. The Accurate Prediction Model of AML was constructed using the following formula: APMAO_i = ∑_(j = 1)^;n▒ 〖factor〗 _ji- 〖 × β_j 〗 . In this formulation, 'factor' represents the score attributed to a specific phenotypic characteristic, β indicates the regression coefficient assigned to each factor as per the regression outcomes, and APMAO is calculated by summing the products of the significantly correlated factor scores and their respective regression coefficients for each sample. In this equation, the index i corresponds to the individual sample, while j represents the specific phenotypic variable under consideration.

To assess the reproducibility and broad applicability of the APMAO model, we incorporated five external GEO datasets for validation purposes (GSE37642 (two platforms: GSE37642-GPL570, GSE37642-GPL96); GSE12417 (two platforms: GSE12417-GPL96, GSE12417-GPL570); GSE10358; GSE146173; and GSE106291) for validation analysis. Considering the potential batch effects between different datasets, we performed validation analyses of the APMAO model respectively for each dataset. The sample sizes and platform information for these datasets are summarized in Table 3. These datasets encompassed a diverse range of platform types (GPL570, GPL96, and GPL18460) and sample sizes (ranging from 79 to 417). Specifically, GSE37642 and GSE12417 each contained

Table 3
Summary of independent GEO datasets used for validation analysis of the APMAO model.

Accession	Sample Count	Platform	Series Type
GSE37642	140	GPL570	Expression profiling by array
	417	GPL96	Expression profiling by array
GSE12417	79	GPL570	Expression profiling by array
	163	GPL96	Expression profiling by array
GSE10358	86	GPL570	Expression profiling by array
GSE146173	246	GPL18460	high throughput sequencing
GSE106291	250	GPL18460	high throughput sequencing

two subsets based on the GPL570 platform (140 and 79 samples, respectively) and the GPL96 platform (417 and 163 samples, respectively). GSE10358 was based on the GPL570 platform and included 86 samples. Both GSE146173 and GSE106291 were based on the GPL18460 platform, with 246 and 250 samples, respectively.

To evaluate the prognostic performance of the APMAO model, we divided the TCGA samples into high and low APMAO score groups using the median score as the cutoff. Kaplan-Meier (KM) survival curves were then generated for these groups using overall survival (OS) data, and a log-rank test was performed to assess the significance of the difference in survival between the high and low APMAO score groups. A p-value <0.05 was considered statistically significant, indicating a meaningful prognostic difference. We then applied the same approach to validate the APMAO model in five independent GEO datasets. Furthermore, to assess the predictive accuracy of the APMAO scores, we calculated the area under the receiver operating characteristic (ROC) curve (AUC) values for predicting 1-year, 3-year, and 5-year survival in both the TCGA and the five GEO validation datasets. The ROC curves were plotted to visualize the performance of the APMAO scores in predicting survival at these time points.

To investigate potential differences in Transcriptional_Score, age, gender, FAB subtype, cytogenetic risk category, FLT3 mutation status, NPM1 mutation status, and RUNX1 mutation status between the high and low APMAO score groups, we conducted differential analyses using the Kruskal-Wallis test for continuous variables and Fisher's exact test for categorical variables. The results of these analyses were visualized using heatmaps to provide a comprehensive overview of the associations between the APMAO score groups and the various clinical and molecular characteristics. Furthermore, we explored the relationships between APMAO scores and each of the aforementioned variables using the Wilcoxon rank-sum test for binary variables (e.g., gender, mutation status) and the Kruskal-Wallis test for variables with more than two categories (e.g., FAB subtype, cytogenetic risk category). Box plots were generated to visually represent the distribution of APMAO scores across the different subgroups defined by these variables, allowing for a clear assessment of the associations between the APMAO score and the clinical and molecular features of the AML samples.

To validate the APMAO model, we first conducted univariate Cox regression analysis on the Transcriptional_Score, age, gender, and FAB classification to identify variables significantly associated with survival. We then performed multivariate Cox regression analysis to confirm that the significant variables included in the APMAO score were independent prognostic factors. The results were visualized using column line plots, which were generated using the R packages rms (version 6.1–0), survival, and regplot (version 1.1). Specifically, we first constructed the Cox proportional hazards regression model using the cph (.) function, then calculated the survival probabilities using the survfit (.) function, and finally created the column line plot using the regplot (.) function to display the calibration curve. To assess the clinical utility of the APMAO model, we performed decision curve analysis (DCA) using the decision_curve (.) function from the R package rmda (version 1.6). The decision curve was plotted to visualize the net benefit of using the APMAO model for making clinical decisions at different threshold probabilities, compared to the strategies of treating all patients or treating none.

2.2. Exploring the molecular underpinnings associated with APMAO scores: insights from mutational profiles and enriched biological pathways

To investigate the mutational landscapes associated with different APMAO score groups, we combined the mutation annotation format (MAF) files for TCGA-LAML samples with the corresponding APMAO group information using the R package maftools. We then identified genes that were mutated in at least one sample and compared the mutation frequencies of these genes between the high and low APMAO score groups. Fisher's exact test was used to assess the statistical significance of the differences in mutation frequencies between the two groups. To explore the biological pathways associated with the APMAO score groups, we performed single-sample gene set enrichment analysis (ssGSEA) using the Hallmark gene sets from the Molecular Signatures Database (MSigDB, version 7.5.1). This analysis yielded enrichment scores for each sample, indicating the extent to which each Hallmark pathway was upregulated or downregulated. Heatmaps were generated to visualize the ssGSEA results, providing an overview of the pathway enrichment patterns across the samples. The Wilcoxon rank-sum test was employed to evaluate the significance of the differences in pathway enrichment scores between the high and low APMAO score groups, enabling the identification of pathways that were differentially activated or suppressed in relation to the APMAO score.

2.3. Evaluation of immune cell infiltration patterns associated with APMAO scores

To investigate the immune cell infiltration patterns associated with APMAO scores, we employed a multi-step approach. First, we utilized the GSVA R package to perform single-sample gene set enrichment analysis (ssGSEA) and quantify the enrichment scores of 28 distinct immune cell subpopulations within the tumor samples. The resulting enrichment scores were then subjected to standardization using the scale (.) function to facilitate comparative analysis. Next, we stratified the samples into high and low APMAO score groups and conducted a comparative assessment of the normalized enrichment scores between these groups. Box plots were generated to visually represent the distribution and differences in immune cell infiltration between the APMAO subgroups. Furthermore, to explore the relationship between APMAO scores and the infiltration levels of specific immune cell types, we calculated the Pearson correlation coefficient between the APMAO scores and the enrichment scores of each immune cell subpopulation. The correlation results were graphically represented using bubble plots to provide a comprehensive overview of the associations between APMAO scores and immune cell infiltration patterns.

2.4. Evaluation of the association between APMAO scores and markers of immunotherapy sensitivity and tumor immune escape

To assess the potential predictive value of APMAO scores in determining the effectiveness of cancer immunotherapy, we conducted a comprehensive analysis of the expression profiles of key immunotherapy-related gene sets, including immune checkpoint genes, interferon-gamma pathway markers, and m6A regulators. Additionally, we examined the relationship between APMAO scores and the Tumor Immune Dysfunction and Exclusion (TIDE) dysfunction scores, which have been previously reported as a measure of tumor immune escape [28]. The interferon-gamma pathway markers and m6A regulators were curated from relevant literature [29]. We employed the Wilcoxon rank-sum test to evaluate the differential expression of these genes between the high and low APMAO score groups within the TCGA-LAML dataset. To further investigate the association between APMAO scores and tumor immune evasion, we obtained the TIDE scores for the TCGA samples from the publicly available TIDE web resource (http://tide.dfci.harvard.edu) and visualized their relationship with APMAO scores using scatter plots. To gain insights into the potential impact of APMAO scores on immunotherapy responses, we leveraged the IMvigor210 bladder cancer dataset, which was accessed using the IMvigor210CoreBiologies R package (v 1.0.0). We calculated transcriptome scores for each sample based on the genes included in our transcriptome score model and stratified the samples into high and low score subgroups using the median score as the cutoff. Kaplan-Meier (KM) curves and receiver operating characteristic (ROC) curves were constructed to evaluate the prognostic and predictive performance of the transcriptome scores in the IMvigor210 dataset. Furthermore, we assessed the differences in transcriptome scores across various response subgroups and visualized these differences using box plots to identify potential associations between the transcriptome scores and immunotherapy response patterns.

3. Results

3.1. Elucidation of putative oncogenic drivers

Through screening of the TCGA-LAML dataset, which comprised expression, phenotype, and survival data for 132 cancer cases, we identified 95 out of 706 cancer-related genes that exhibited significant associations with survival ($p < 0.05$) using univariate Cox regression analysis (Supplementary Table 1). To validate these findings, we employed the independent GSE37642 dataset and found that 9 of the 95 genes consistently demonstrated significant associations with survival in both datasets (Supplementary Table 2). These

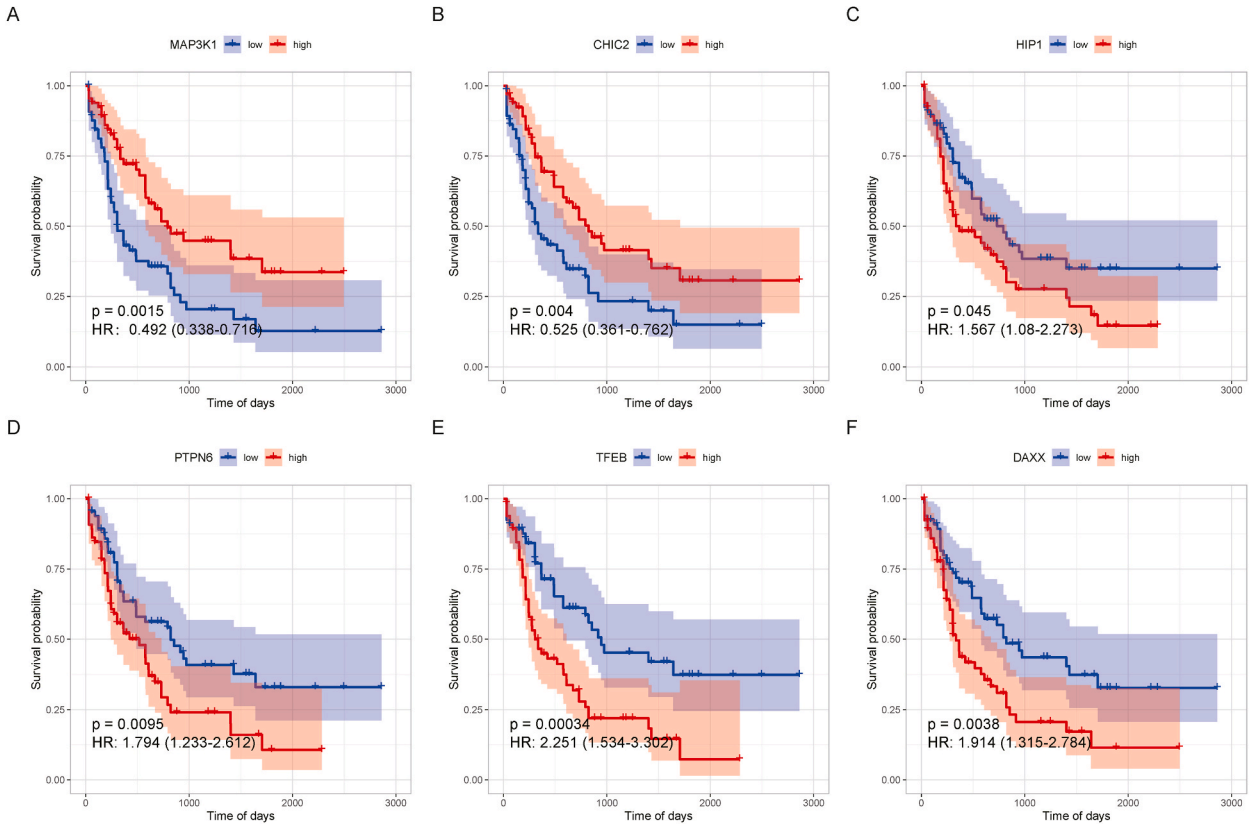

Fig. 1. Kaplan-Meier survival curves for the 6 primary effector genes identified through LASSO regression analysis. (A) MAP3K1, (B) CHIC2, (C) HIP1, (D) PTPN6, (E) TFEB, and (F) DAXX.

9 genes were designated as primary effectors for further investigation. To elucidate the interactions among driver genes in cancer, we computed Pearson correlation coefficients for all possible gene pairs within the TCGA dataset and identified 3793 gene pairs that displayed strong reciprocal relationships ($|cor| > 0.6$ and adjusted p-value <0.05; Supplementary Table 3). We then validated these gene pairs using the GSE37642 dataset, revealing 313 gene pairs that exhibited robust interactions in both datasets, encompassing a total of 192 genes (Supplementary Table 4). The amalgamation of the essential effector and interacting genes led to the compilation of a final set of 200 genes. Utilizing LASSO regression for refinement, 7 genes were selected, namely ACSL6, MAP3K1, CHIC2, HIP1, PTPN6, TFEB, and DAXX. Among these, MAP3K1, CHIC2, HIP1, PTPN6, TFEB, and DAXX functioned as main effector genes, while TFEB and PTPN6 served as interacting genes. Notably, ACSL6 displayed significant reciprocal interactions with non-model genes (ACSL6-ANK1). Comprehensive graphical depictions of the data are presented in Figs. 1 and 2, as well as Supplementary Fig. 1, providing a visual reference for the findings.

Fig. 1 presents the Kaplan-Meier survival curves for the six primary effector genes identified through LASSO regression analysis. Fig. 1A shows that higher expression of MAP3K1 (red line) is significantly associated with better prognosis in AML compared to lower expression (blue line), with a p-value of 0.0015. Similarly, Fig. 1B demonstrates that higher expression of CHIC2 (red line) correlates with a significantly higher survival probability than lower expression (blue line), with a p-value of 0.004. In contrast, Fig. 1C reveals that lower expression of HIP1 (blue line) is associated with a significantly higher survival probability compared to higher expression (red line), with a p-value of 0.045. Fig. 1D indicates that lower expression of PTPN6 (blue line) correlates with a significantly higher survival probability than higher expression (red line), with a p-value of 0.0095. Similarly, Fig. 1E shows that lower expression of TFEB (blue line) is linked to a significantly higher survival probability compared to higher expression (red line), with a p-value of 0.00034. Finally, Fig. 1F reveals that lower expression of DAXX (blue line) is associated with a significantly higher survival probability than higher expression (red line), with a p-value of 0.0038. In summary, the Kaplan-Meier curves in Fig. 1 demonstrate that higher expression of MAP3K1 and CHIC2 is significantly associated with better prognosis in AML, while lower expression of HIP1, PTPN6, TFEB, and DAXX correlates with improved survival outcomes.

Fig. 2 illustrates the strongly interacting gene pairs selected using LASSO regression analysis. Fig. 2A presents a scatter plot showing a significant positive correlation between the expression levels of PTPN6 and TFEB, with a Pearson correlation coefficient (R) of 0.649 and a p-value of 0.001. Similarly, Fig. 2B demonstrates a significant positive correlation between the expression levels of ACSL6 and ANK1, with a Pearson correlation coefficient (R) of 0.680 and a p-value less than 0.001. These findings suggest that PTPN6 and TFEB, as well as ACSL6 and ANK1, are strongly interacting gene pairs in AML, which may have important implications for understanding the molecular mechanisms underlying the disease and developing targeted therapies.

Accurate Prediction Model of AML Overall Survival (APMAO) Score: Development, Validation, and Integration of Clinical and Transcriptomic Features.

A transcriptional score was constructed using the correlation coefficients of two genes (MAP3K1 and TFEB): Transcriptional_Score $= (-0.5248) * MAP3K1 + 0.4144 * TFEB$. This score quantifies the combined prognostic impact of MAP3K1 and TFEB in AML.

The selection of variables for the multivariate Cox regression analysis was guided by their statistical significance in univariate Cox regression and their anticipated clinical relevance. The coefficients (coef) were employed as weights for each chosen variable in the APMAO model, thereby reflecting their relative contribution to the prediction of overall survival. Table 4 presents the coef values for the selected variables, providing a quantitative measure of their impact on the prognostic model.

To develop the APMAO score, we conducted a multivariate Cox regression analysis incorporating the Transcriptional_Score, age, gender, and French-American-British (FAB) classification as potential predictors of overall survival in AML patients. The results of this

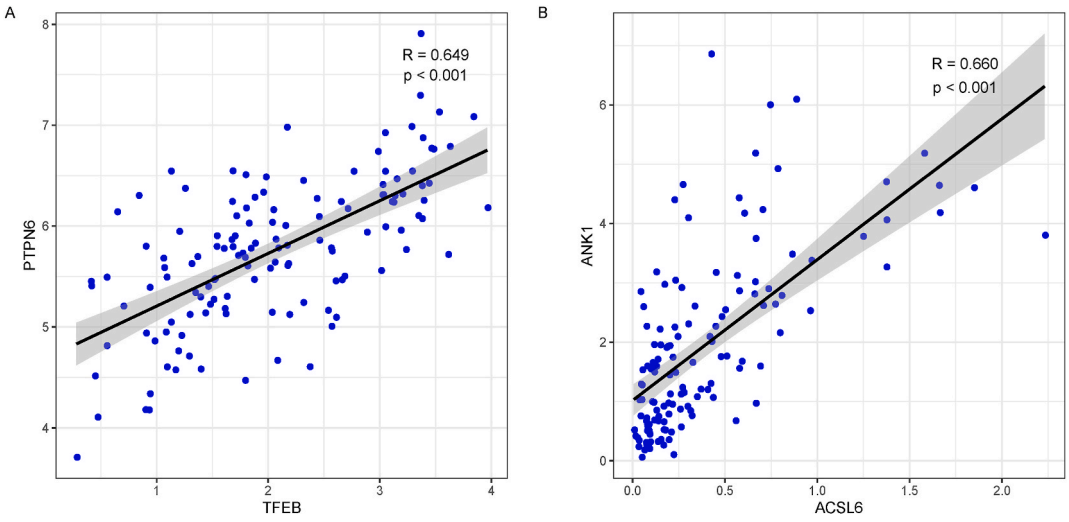

Fig. 2. Scatter plots depicting the expression levels of strongly interacting gene pairs identified through LASSO regression analysis. (A) PTPN6 and TFEB and (B) ACSL6 and ANK1.

Table 4
Multivariate Cox regression analysis results for the selected cancer driver genes, presenting the regression coefficients (coef), hazard ratios (HR), p-values, and 95 % confidence intervals (CIL and CIU) for each gene. The coef values indicate the relative weights assigned to each gene in the APMAO model, reflecting their contribution to overall survival prediction. Genes with p-values <0.05 are considered statistically significant predictors of survival in this multivariate context.

	coef	HR	p	CIL	CIU
ACSL6	−0.57084	0.565052	0.059941	0.343026	0.930787
CHIC2	−0.36312	0.695503	0.359725	0.362312	1.335105
DAXX	0.892136	2.440338	0.080379	1.054303	5.648516
HIP1	0.141611	1.152129	0.3124	0.914876	1.450907
MAP3K1	−0.52483	0.591657	0.006268	0.431431	0.811388
PTPN6	0.061711	1.063655	0.779284	0.74046	1.527917
TFEB	0.414358	1.513399	0.026087	1.114078	2.055849

analysis identified the Transcriptional_Score and age as statistically significant predictors of survival outcomes. Based on these findings, we constructed the final APMAO score using the following formula: APMAO = 1.2898 * Transcriptional_Score +0.0273 * age.

Fig. 3 demonstrates the prognostic efficacy of the transcriptional score and APMAO score in the TCGA dataset (Fig. 3A and B) and multiple independent GEO datasets (GSE37642-GPL570 (Fig. 3C and D), GSE37642-GPL96 (Fig. 3E and F), GSE10358 (Fig. 3G and H), GSE106291 (Fig. 3I and J), GSE146173 (Fig. 3K and L), GSE12417-GPL570 (Fig. 3M and N), and GSE12417-GPL96 (Fig. 3O and P)). Across most of the datasets included in our analysis, we observed that the survival curves for patients stratified into high and low transcriptional score groups, as well as those stratified into high and low APMAO score groups, displayed statistically significant differences ($p < 0.05$). However, the transcriptional score failed to achieve statistical significance in differentiating survival outcomes in several datasets, including GSE10358 ($p = 0.83$, Fig. 3G), GSE106291 ($p = 0.19$, Fig. 3I), GSE146173 ($p = 0.46$, Fig. 3K), GSE12417-GPL570 ($p = 0.95$, Fig. 3M), and GSE12417-GPL96 ($p = 0.13$, Fig. 3O). The APMAO score exhibited a remarkable consistency in its prognostic performance, showing statistically significant differences between high and low-risk groups across all datasets analyzed ($p < 0.05$, Fig. 3B–D, F, H, J, L, N, P). These findings suggest that the integration of the transcriptional score with clinical indicators in the APMAO score may confer enhanced robustness and generalizability in predicting AML prognosis compared to the transcriptional score alone. Despite the limitations observed in certain datasets, the APMAO score exhibits superior performance as a prognostic marker for AML, highlighting the importance of incorporating both transcriptomic and clinical data in prognostic model development.

Fig. 4 presents the ROC curves of the APMAO score for predicting survival in various datasets. The APMAO score exhibited robust prognostic prediction performance across the TCGA dataset (Fig. 4A) and several independent GEO datasets, including GSE37642-GPL570 (Fig. 4B), GSE37642-GPL96 (Fig. 4C), GSE10358 (Fig. 4D), GSE106291 (Fig. 4E), GSE146173 (Fig. 4F), GSE12417-GPL570 (Fig. 4G), and GSE12417-GPL96 (Fig. 4H). To evaluate the predictive performance of the APMAO score, we generated ROC curves and calculated the area under the curve (AUC) values for 1-year, 3-year, and 5-year survival predictions across the TCGA and independent GEO datasets. Remarkably, the AUC values consistently exceeded 0.6 in all datasets, underscoring the robust predictive capacity of the APMAO score. Of particular note, the AUC for predicting 5-year survival attained an impressive 0.94 in the TCGA dataset (Figs. 4A) and 0.84 in the GSE10358 dataset (Fig. 4D), highlighting the exceptional long-term prognostic value of the APMAO score in these cohorts. These results support the reliability and versatility of the APMAO score as a prognostic assessment tool for AML across different datasets and platforms.

The robust performance and broad applicability of the APMAO model were thoroughly validated using rigorous statistical analyses in each independent dataset (Table 5). Kaplan-Meier survival curves consistently demonstrated significant differences in survival outcomes between the high and low APMAO score groups, with log-rank test *P*-values remaining below the 0.05 significance threshold across all datasets. Remarkably, the GSE37642-GPL570, GSE37642-GPL96, GSE10358, GSE146173, and GSE106291 datasets demonstrated exceptionally low *P*-values (<0.0001), underscoring the robust predictive capacity of the APMAO score in determining survival outcomes. Furthermore, receiver operating characteristic (ROC) curve analysis provided compelling evidence for the strong predictive capability of the APMAO score across all validation datasets. The area under the curve (AUC) values for predicting 1-year, 3-year, and 5-year survival rates consistently surpassed 0.6 in each dataset, signifying good predictive performance. Remarkably, the GSE37642-GPL570, GSE37642-GPL96, and GSE10358 datasets exhibited exceptional predictive power, with AUC values spanning an impressive range from 0.7 to 0.84. However, due to the absence of 5-year survival data in the GSE12417-GPL96 and GSE12417-GPL570 datasets, the assessment of AUC values for 5-year survival rates was not feasible. The APMAO model demonstrated consistent predictive utility, with AUC values for 1-year and 3-year survival rates consistently exceeding the 0.6 threshold. These findings collectively emphasize the robustness and generalizability of the APMAO model in predicting survival outcomes across diverse AML patient cohorts.

In the TCGA dataset, notable distinctions were observed between the high and low APMAO subgroups concerning Transcriptional_Score, age, cytogenetic_risk_category, and FAB parameters (Fig. 5). Conversely, significant differences in mean APMAO scores were identified among age, cytogenetic_risk_category, and Transcriptional_Score subgroups (Fig. 6). Fig. 6 illustrates the differences in APMAO scores across subgroups defined by various phenotypic variables in the TCGA dataset. Fig. 6A shows that patients aged >65 years have significantly higher APMAO scores compared to those aged ≤65 years ($p < 0.001$). Fig. 6B reveals no significant difference in APMAO scores between male and female patients ($p = 0.78$). Fig. 6C demonstrates no significant differences in APMAO scores among different FAB classification subgroups (ns). Fig. 6D indicates significant differences in APMAO scores across cytogenetic risk categories, with the intermediate/normal and poor risk groups having higher scores compared to the favorable risk group, while

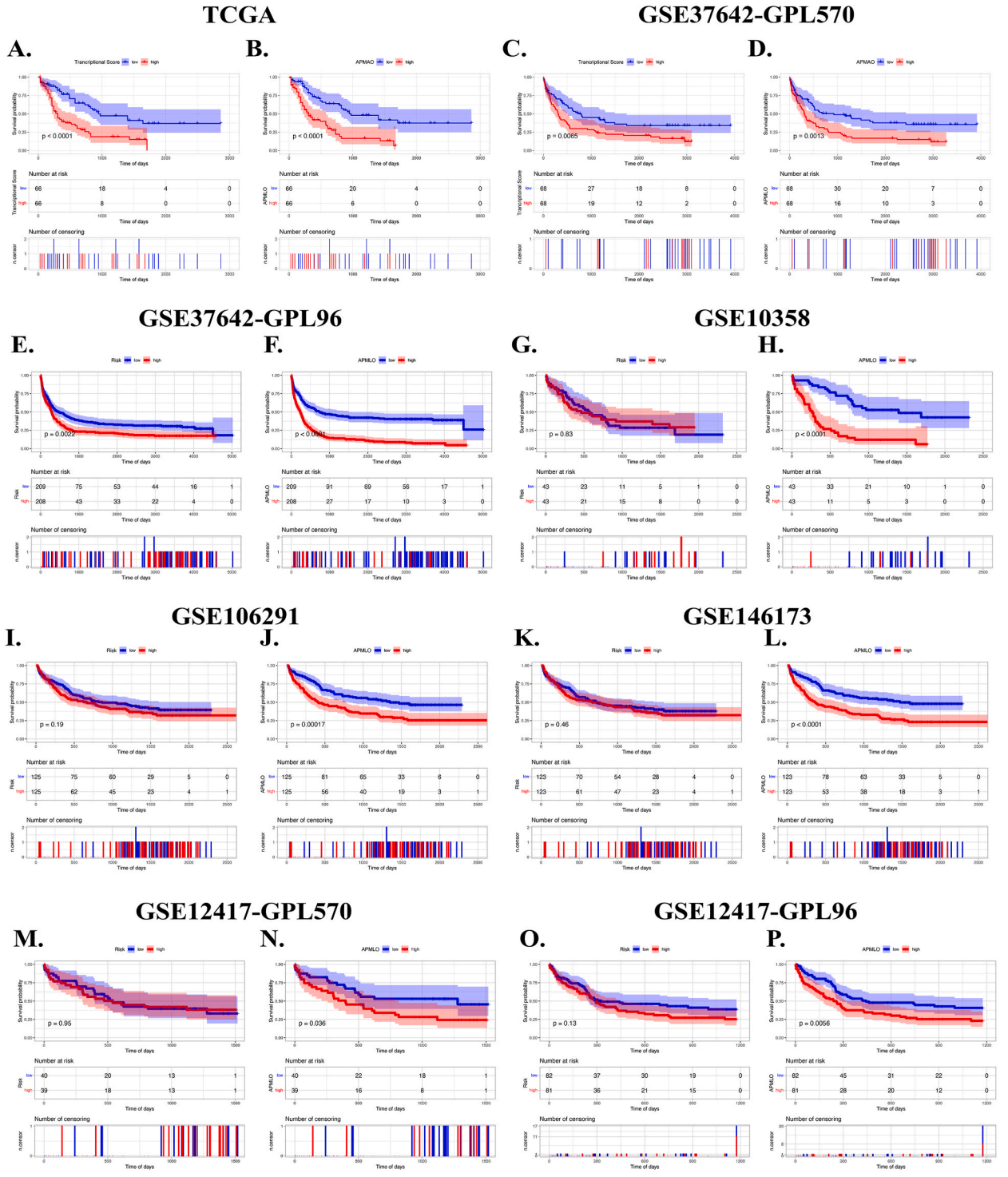

Fig. 3. Kaplan-Meier survival curves demonstrating the prognostic value of the transcriptional score and APMAO score in predicting overall survival (OS) for acute myeloid leukemia (AML) patients across diverse datasets. The datasets include TCGA (A, B), GSE37642-GPL570 (C, D), GSE37642-GPL96 (E, F), GSE10358 (G, H), GSE106291 (I, J), GSE146173 (K, L), GSE12417-GPL570 (M, N), and GSE12417-GPL96 (O, P). In each dataset, patients are stratified into high and low score groups based on the median value of the respective score (transcriptional score or APMAO score).

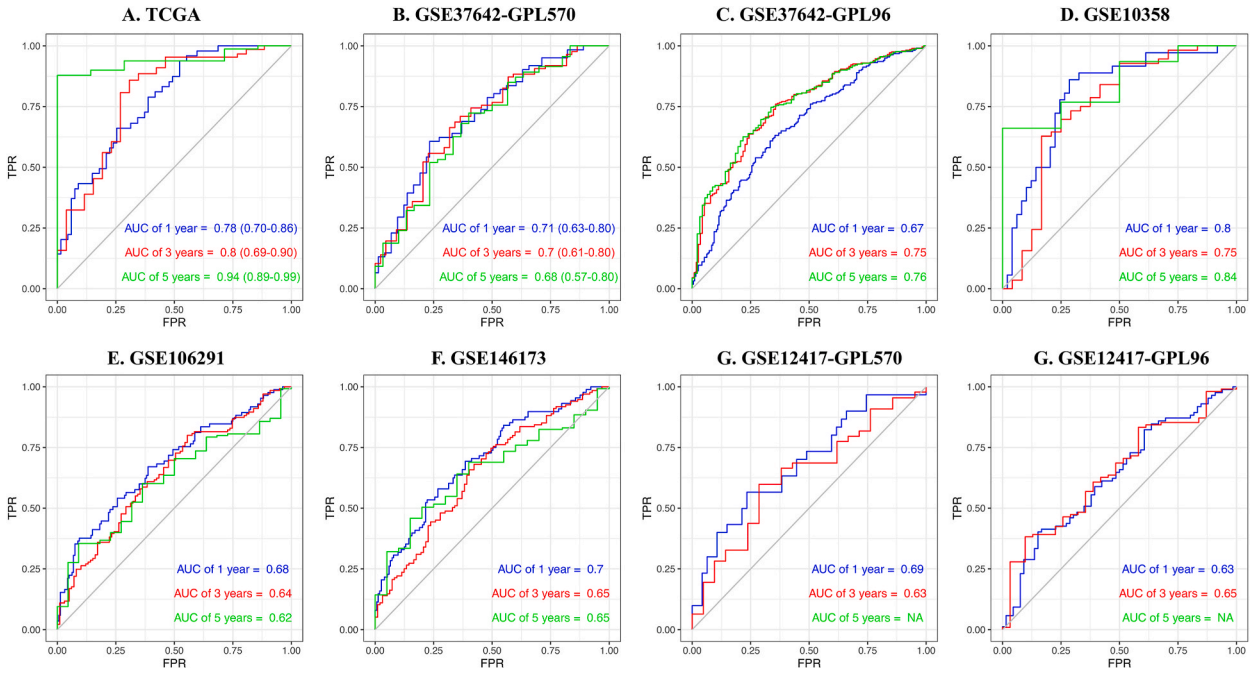

Fig. 4. Receiver operating characteristic (ROC) curves illustrating the predictive performance of the APMAO score for 1-year, 3-year, and 5-year survival rates in the TCGA dataset (A) and multiple independent GEO datasets, including GSE37642-GPL570 (B), GSE37642-GPL96 (C), GSE10358 (D), GSE106291 (E), GSE146173 (F), GSE12417-GPL570 (G), and GSE12417-GPL96 (H). The ROC curves plot the true positive rate (sensitivity) against the false positive rate (1-specificity) at various threshold settings for the APMAO score.

Table 5
Comprehensive assessment of the APMAO model's performance in independent validation cohorts. The table summarizes the results of Kaplan-Meier (KM) survival analysis, depicting the statistical significance of survival differences between high and low APMAO score groups, and receiver operating characteristic (ROC) curve analysis, presenting the area under the curve (AUC) values for predicting 1-year, 3-year, and 5-year survival rates in each dataset.

Datasets	KM-pvalue	1year	3years	5years
TCGA-AML	<0.0001	0.78	0.8	0.94
GSE37642-GPL570	<0.0001	0.71	0.7	0.68
GSE37642-GPL96	<0.0001	0.67	0.75	0.76
GSE12417-GPL96	0.0056	0.63	0.65	NA
GSE12417-GPL570	0.036	0.69	0.63	NA
GSE10358	<0.0001	0.8	0.75	0.84
GSE146173	<0.0001	0.7	0.65	0.65
GSE106291	0.00017	0.68	0.64	0.62

no significant difference is observed between the intermediate/normal and poor risk groups. Fig. 6E and F show no significant differences in APMAO scores between FLT3 (Fig. 6E) or NPM1 (Fig. 6F) mutation status subgroups (mut vs. wt), respectively. Similarly, Fig. 6G reveals no significant difference in APMAO scores between RUNX1 mutation status subgroups (mut vs. wt). Finally, Fig. 6H demonstrates that the high Transcriptional_Score group has significantly higher APMAO scores compared to the low Transcriptional_Score group ($p < 0.001$, ***).

Univariate and multivariate Cox regression analyses were performed to assess the prognostic significance of the APMAO score components in predicting overall survival (OS) for the TCGA-LAML dataset (Fig. 7). The results of these analyses consistently demonstrated that both the Transcriptional_Score and age were significant independent prognostic factors, with p-values below the 0.05 threshold. Moreover, decision curve analysis demonstrated that Transcriptional_Score had a higher net benefit compared to other variables, highlighting its superior decision-making efficacy and importance as a key determinant (Fig. 8).

Fig. 8 demonstrates the performance of the multivariate Cox regression model incorporating the Transcriptional_Score. Fig. 8A presents a nomogram plot that allows for the calculation of a total score based on the Transcriptional_Score, age, and FAB classification, which can then be used to predict survival probabilities. Fig. 8B shows the calibration curves comparing the predicted and observed survival rates at 1-year, 3-year, and 5-year time points, demonstrating good calibration of the model. Fig. 8C–E displays the decision curves, which reveal that using the model for treatment decisions provides a positive net benefit across a wide range of threshold probabilities, outperforming the treat-all/none strategies for 1-year, 3-year, and 5-year survival predictions. These findings

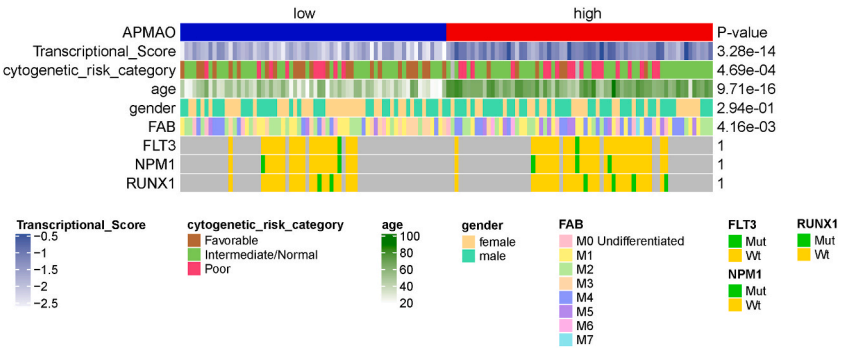

Fig. 5. Heatmap depicting the differences in phenotypic variables and gene expression levels between the high and low APMAO score groups in the TCGA dataset. Rows represent specific variables or genes, while columns correspond to individual patient samples. Color intensity reflects the value of each variable or gene expression level, with red indicating higher values and blue indicating lower values. The heatmap reveals distinct patterns of association between the APMAO score and variables such as Transcriptional_Score, age, cytogenetic_risk_category, FAB classification, and expression levels of FLT3, NPM1, and RUNX1.

collectively highlight the good predictive performance of the multivariate model and the importance of the Transcriptional_Score as a key predictor strongly associated with survival outcomes.

3.2. Mutational landscape and enriched pathways associated with APMAO scores

To gain insights into the mutational profiles associated with the APMAO score, we performed a comprehensive analysis of the mutational landscape in TCGA samples stratified by high and low APMAO scores (Fig. 9, Supplementary Table 5). Notably, the overall mutation frequency was moderately elevated in the high APMAO group (74.19 %) compared to the low APMAO group (72.73 %). Intriguingly, the DNMT3A gene emerged as the most frequently mutated gene in the high APMAO group, with a mutation rate of 13 %. In contrast, the TTN gene exhibited the highest mutation rate of 14 % in the low APMAO group. These findings suggest that distinct mutational patterns may underlie the biological differences between high and low APMAO score subgroups. Supplementary Table 5 presents a detailed overview of the mutation rate differences across all genes between the high and low APMAO subgroups, offering a comprehensive resource for further exploration of the genetic alterations associated with the APMAO score in AML.

Fig. 9 illustrates the mutational landscape of acute myeloid leukemia (AML) samples from The Cancer Genome Atlas (TCGA) stratified by APMAO (Accurate Prediction Model of AML Overall Survival) scores. Fig. 9A depicts the mutation profiles of the high APMAO score group. In this group, DNMT3A (13 %), RUNX1 (13 %), and TP53 (13 %) emerge as the most frequently mutated genes, followed by BPIFC (10 %), BSN (10 %), IDH2 (10 %), KRAS (10 %), and NPM1 (10 %). Fig. 9B shows the mutation profiles of the low APMAO score group. TTN (14 %) appears as the most frequently mutated gene in this group, followed by ADAMTS19 (9 %), BPIFC (9 %), C10orf71 (9 %), CWCH43 (9 %), DDX52 (9 %), DNAH11 (9 %), DNMT3A (9 %), GPR112 (9 %), HPS3 (9 %), and ITGA1 (9 %). In summary, Fig. 9 highlights the differences in the mutational landscapes between the high and low APMAO score groups, with specific genes showing distinct mutation frequencies in each group. These findings suggest that different genetic alterations may be associated with varying prognostic outcomes in AML patients, as captured by the APMAO scoring system.

To elucidate the functional pathways associated with the APMAO score, we performed an enrichment analysis using the hallmark gene sets from the MSigDB database. Remarkably, 35 out of the 50 pathways examined showed significant differences in enrichment scores between the high and low APMAO groups. Notably, several pathways were found to be significantly upregulated in the high APMAO group compared to the low APMAO group. These included TNF-α signaling via NF-κB, hypoxia, IL-6/JAK/STAT3 signaling, complement activation, Notch signaling, and allograft rejection pathways. The enhanced activation of these pathways in the high APMAO group suggests that they may play crucial roles in driving the aggressive phenotype and poor prognosis associated with high APMAO scores. In contrast, the high APMAO group demonstrated significantly lower enrichment scores for the MYC targets V1 and unfolded protein response pathways relative to the low APMAO group. These findings are visually represented in Fig. 10, which highlights the distinct pathway enrichment patterns associated with the APMAO score subgroups.

3.3. Immune cell infiltration patterns linked to APMAO scores

Among the 28 distinct immune cell populations evaluated, 20 exhibited significant variations in their enrichment scores across the APMAO groups. Notably, the high APMAO score cohort demonstrated elevated enrichment levels for several crucial immune cell types, including central memory $CD4^+$ T lymphocytes, γδ T cells, immature B cells, T follicular helper cells, activated dendritic cells, CD56dim natural killer cells, macrophages, natural killer T cells, and plasmacytoid dendritic cells, when compared to their low APMAO score counterparts. To further elucidate the relationship between the APMAO score and the immune landscape, we performed correlation analyses between the APMAO scores and the enrichment profiles of the infiltrating immune populations. These analyses revealed a significant positive correlation between elevated APMAO scores and heightened enrichment of activated dendritic cells, macrophages, myeloid-derived suppressor cells (MDSCs), natural killer cells, plasmacytoid dendritic cells, and T follicular helper cells,

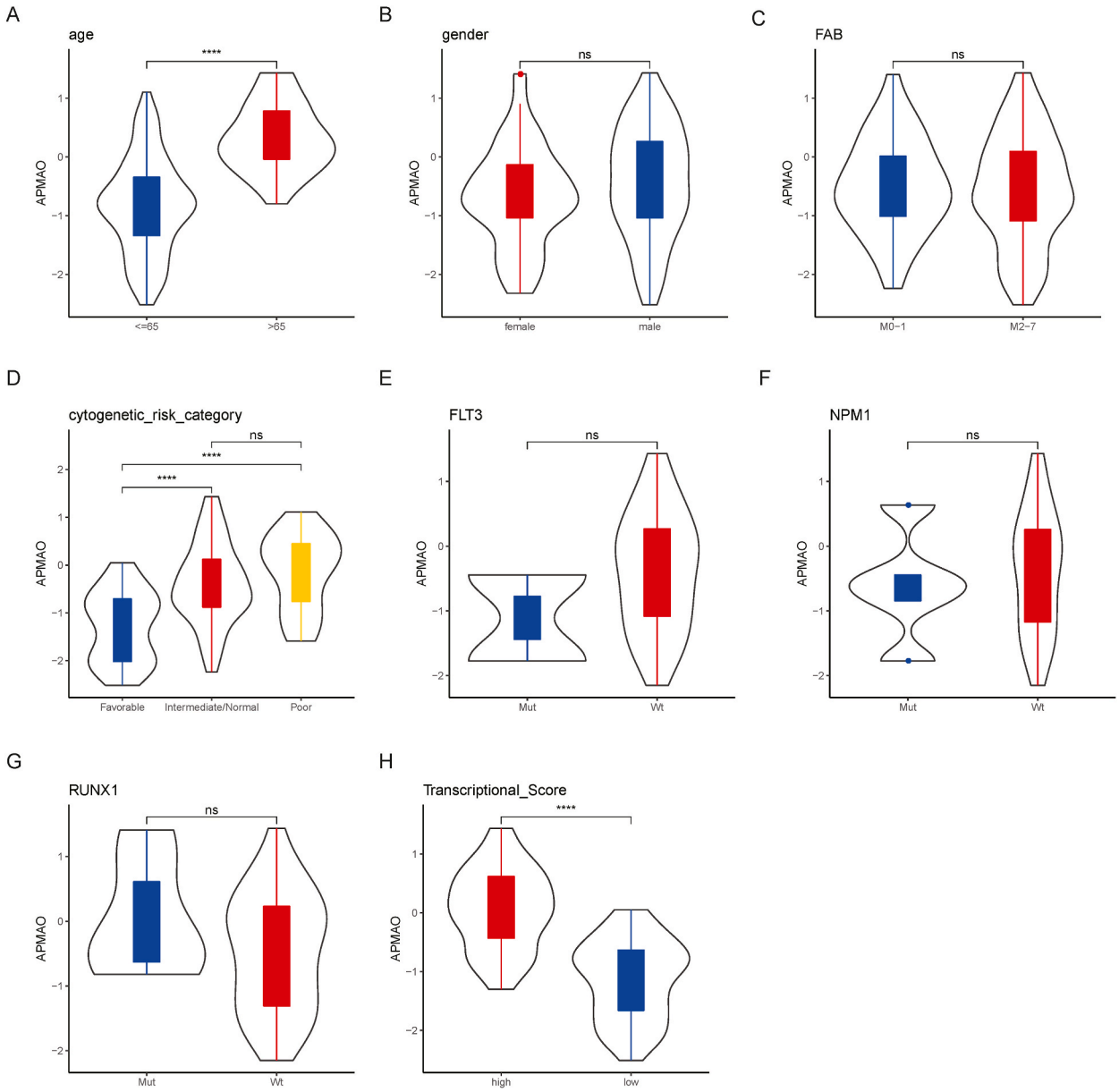

Fig. 6. The differences in APMAO scores across subgroups defined by various phenotypic variables in the TCGA dataset. The box plots compare APMAO scores between subgroups based on age (A), gender (B), FAB classification (C), cytogenetic risk category (D), FLT3 mutation status (E), NPM1 mutation status (F), RUNX1 mutation status (G), and Transcriptional_Score (H).

as depicted in Fig. 11.

Fig. 11 illustrates the immune cell infiltration patterns associated with APMAO scores in acute myeloid leukemia (AML) samples. Fig. 11A presents a heatmap depicting the differences in enrichment scores of 28 immune infiltrating cell types between the high and low APMAO score groups. Each row represents a specific immune cell type, while each column corresponds to an individual patient sample. The color intensity of each cell reflects the enrichment score of the corresponding immune cell type in that particular sample, with red indicating higher enrichment and blue indicating lower enrichment. The heatmap reveals distinct patterns of immune cell infiltration between the high and low APMAO score groups. Notable differences can be observed in the enrichment of activated B cells, activated CD8 T cells, central memory CD4 T cells, central memory CD8 T cells, effector memory CD8 T cells, gamma delta T cells, immature B cells, regulatory T cells, T follicular helper cells, type 1 T helper cells, activated dendritic cells, CD56dim natural killer cells, eosinophils, macrophages, MDSCs, monocytes, natural killer cells, neutrophils, and plasmacytoid dendritic cells, which appear to be more highly enriched in the high APMAO score group compared to the low APMAO score group. Fig. 11B presents a bubble plot illustrating the correlation between APMAO scores and the enrichment scores of various immune infiltrating cell types. Only two cell

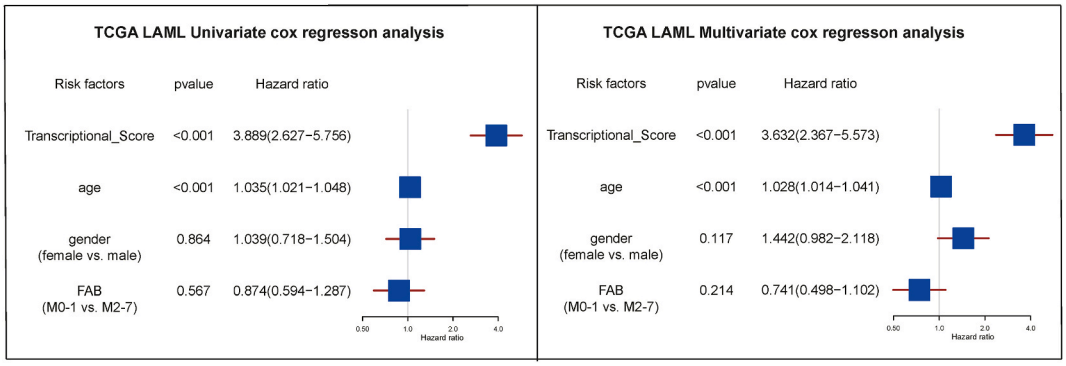

Fig. 7. Forest plots visualizing the results of univariate (left) and multivariate (right) Cox regression analyses, evaluating the prognostic significance of the APMAO score components in predicting overall survival (OS) for the TCGA-LAML dataset. The plots display the hazard ratios (HR) and 95 % confidence intervals (CI) for each variable, with the size of the squares proportional to the variable's weight in the model.

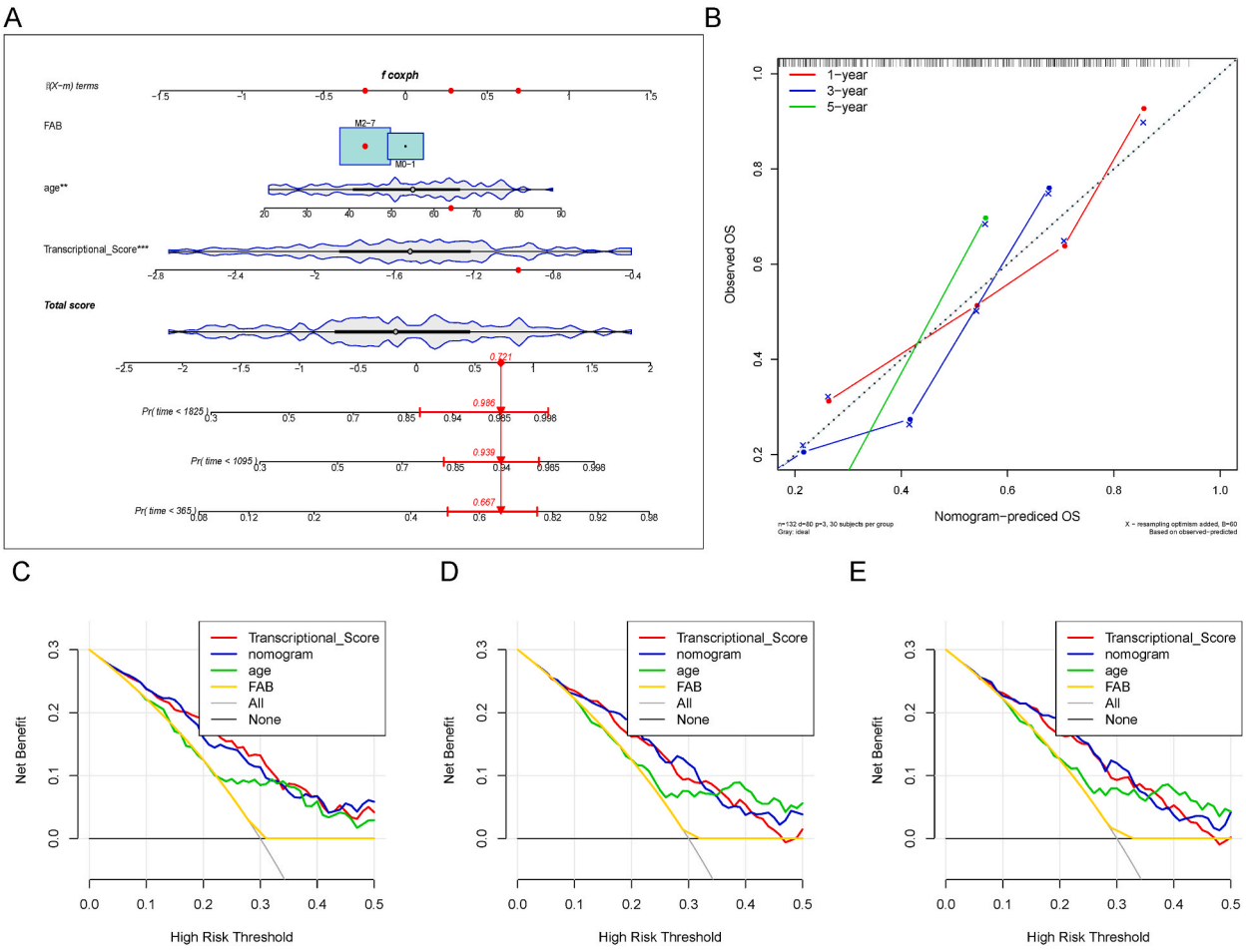

Fig. 8. Evaluation of the multivariate Cox regression model incorporating the Transcriptional_Score using decision curve analysis. (a) Nomogram plot depicting the relationship between the Transcriptional_Score, age, FAB classification, and predicted survival probabilities at different time points. (b) Calibration curves assessing the agreement between predicted and observed survival rates at 1-year, 3-year, and 5-year timepoints, indicating good calibration of the model. (*c*–e) Decision curves displaying the net benefit of using the model for clinical decision-making across a range of threshold probabilities for 1-year (c), 3-year (d), and 5-year (e) overall survival (OS).

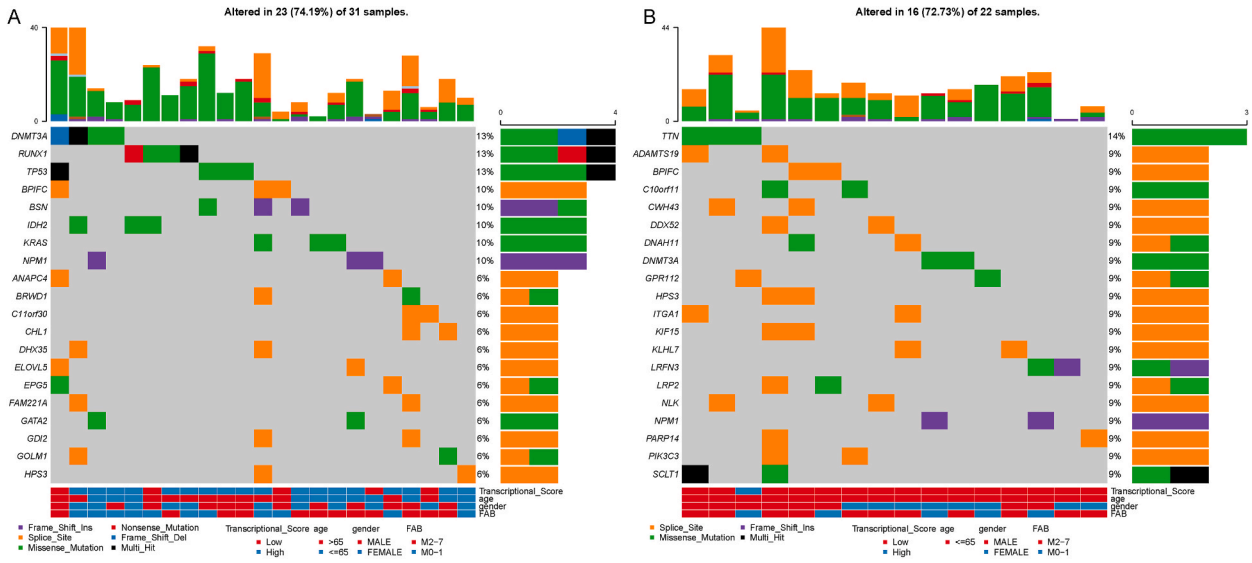

Fig. 9. Mutational landscape of TCGA-LAML samples stratified by APMAO scores. (A) Mutation profiles of the high APMAO score group, with DNMT3A, RUNX1, and TP53 being the most frequently mutated genes. (B) Mutation profiles of the low APMAO score group, with TTN being the most frequently mutated gene. Each row represents a specific gene, and each column corresponds to an individual patient sample. Colored cells indicate the presence of a mutation in the corresponding gene for that particular sample.

types exhibit negative correlations with APMAO scores: memory B cells and CD56bright natural killer cells. All other immune cell types shown in the plot demonstrate positive correlations with APMAO scores, albeit with varying magnitudes. The immune cell types that exhibit positive correlations with APMAO scores include activated dendritic cells, macrophages, MDSCs (myeloid-derived suppressor cells), natural killer cells, plasmacytoid dendritic cells, T follicular helper cells, activated B cells, activated CD4 T cells, activated CD8 T cells, central memory CD4 T cells, central memory CD8 T cells, effector memory CD4 T cells, effector memory CD8 T cells, gamma delta T cells, immature B cells, immature dendritic cells, neutrophils, type 1 T helper cells, type 17 T helper cells, CD56dim natural killer cells, eosinophils, monocytes, mast cells, natural killer T cells, regulatory T cells, and type 2 T helper cells.

3.4. Relationship between APMAO scores and markers of immunotherapy sensitivity and tumor immune escape

Among the 45 checkpoint genes analyzed, 28 exhibited significant differential expression between the high and low APMAO score groups. Notably, elevated APMAO scores were accompanied by heightened expression levels of CD200R1, CD27, CD276, CD40, CD86, PDCD1 (encoding PD-1), PDCD1LG2 (encoding PD-L2), TNFSF14, and TNFSF15. Conversely, the CD160 gene displayed significantly upregulated expression in the low APMAO score subset compared to its high APMAO counterpart, as depicted in Fig. 12.

Turning our attention to interferon-γ pathway markers, we observed significant differential expression in 7 out of the 13 markers examined. IFNGR1, IFNGR2, PTPN1, PTPN6, and SOCS1 displayed increased expression levels in the high APMAO group, whereas PIAS1 and PTPN11 showed higher expression in the low APMAO group, as depicted in Fig. 13. Furthermore, our analysis of m6A regulators revealed differential expression in 9 out of 19 genes between APMAO groups. EIF3A, FTO, HNRNPA2B1, METTL16, YTHDC1, YTHDF2, YTHDF3, and ZC3H13 exhibited significantly higher expression in the low APMAO subgroup, while IGF2BP3 showed significantly elevated expression in the high APMAO subgroup, as presented in Fig. 14.

4. Discussion

In this study, we developed and validated a comprehensive scoring system, termed APMAO, for predicting prognosis in acute myeloid leukemia (AML) by integrating cancer driver genes, phenotypic characteristics, and clinical information. Additionally, we explored the potential utility of the APMAO scoring system in predicting responses to cancer immunotherapy. Initially, we identified a 7-gene prognostic signature for AML, which included ACSL6, MAP3K1, CHIC2, HIP1, PTPN6, TFEB, and DAXX. Previous literature supports the role of several of these genes as oncogenic drivers in AML. For instance, the ETV6ACSL6 rearrangement has been implicated in the pathogenesis of leukemia [30]. The activation of the MAP3K1 kinase has been implicated as a contributing factor in the pathogenesis of various malignant neoplasms, rendering it a prospective therapeutic target, particularly in the context of acute myeloid leukemia (AML) [31]. Aberrations in CHIC2 including TV6/CHIC2 gene fusion resulting in AML have been reported [32,33]. HIP1 regulates endocytosis and is associated with several cancers, and its expression level has been shown as predictor of survival in AML [34]. The posttranscriptional deregulation of the PTPN6 gene that regulates hematopoietic cell development has been implicated in leukemeogenesis [35,36]. TEFB is a transcriptional factor involved in elongation by RNA polymerase II and is a target for AML therapy [37]. The DAXX orphan receptor gene has been implicated in a number of cancer types [38]. Through the application of

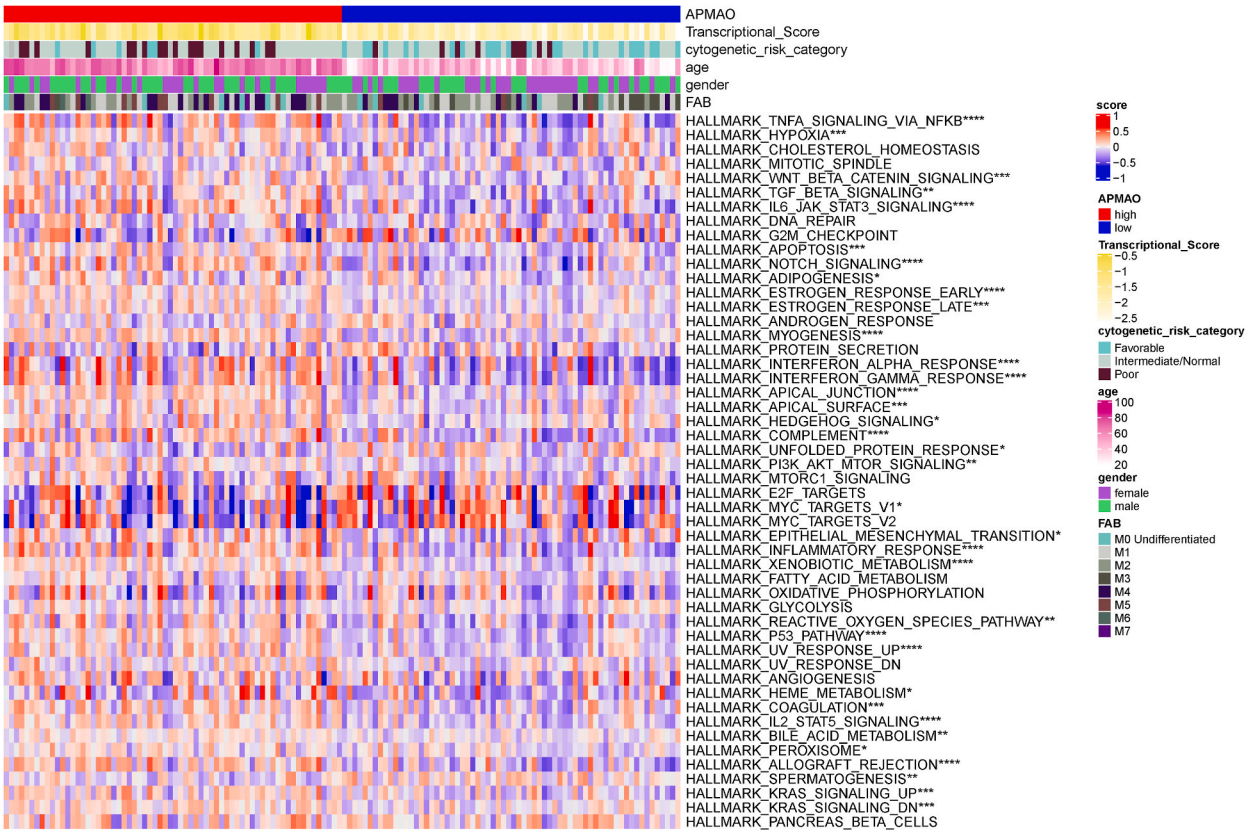

Fig. 10. Heatmap illustrating the differences in hallmark pathway enrichment scores between the high and low APMAO score groups. Rows represent specific hallmark pathways, while columns correspond to individual patient samples. The color intensity of each cell indicates the enrichment score of the corresponding pathway in that particular sample, with red denoting higher enrichment and blue denoting lower enrichment. Asterisks on the right side of the heatmap mark pathways with significantly different enrichment scores between the high and low APMAO groups, with the significance level indicated as follows: ****$p < 0.0001$; ***$p < 0.001$; **$p < 0.01$; *$p < 0.05$.

multivariate Cox regression analysis, two genes from the initial set, namely MAPK31 and TEFB, were selected for the computation of the Transcriptional_Score. The APMAO score was subsequently generated by integrating the selected clinical variable, age, with the Transcriptional_Score. This APMAO score demonstrated a strong discriminative ability in predicting survival outcomes for AML patients, although the 5-year area AUC value was higher for the TCGA dataset compared to the GSE37642 data. Interestingly, while the cytogenetic risk category exhibited a significant association with the APMAO score, it did not emerge as a significant factor in the regression analysis and was not included as a component of the APMAO score. Applying consensus clustering to identify subgroups and LASSO Cox regression, Chen et al. [39] identified a 4 gene prognostic signature of AML comprising KLF9, ENPP4, TUBA4A and CD247 genes that was independent of cytogenetic risk category. The present study did not take into account subgroups based on transcriptional heterogeneity. The European LeukemiaNet has categorized risk categories into 3 levels based on cytogenetics [6] and has been validated [40]. The APMAO score effectively differentiated between the favorable cytogenetic risk category and the intermediate and poor risk categories. Analysis of the mutational profiles associated with varying levels of the APMAO score unveiled an enrichment of DNMT3A mutations among patients exhibiting a high APMAO score stratum. Consistently, earlier works has shown that DNMT3A, a methyltransferase gene that affects translation has a high mutation rate in de-novo AML, and is associated with worse prognosis [41]. Salient observation was the association between lower APMAO scores and the presence of mutations in the TTN gene, which has previously been implicated in prolonged progression-free survival and favorable responses to immune checkpoint inhibitor therapy in solid malignancies [42]. Despite the limited characterization of the implications of TTN mutations in acute myeloid leukemia (AML), the subgroup with elevated APMAO scores demonstrated enrichment across multiple oncogenic signaling cascades, encompassing the NFκB, TNF, IL-6, hypoxia, complement, JAK-STAT3, and NOTCH pathways. In contrast, the MYC target V1 and unfolded protein response pathways were comparatively downregulated in this subgroup. Previous studies have identified MYC protein expression as a prognostic factor in AML and a potential therapeutic target, with higher levels of MYC immunopositivity associated with poorer outcomes in older patients and those with higher-risk disease [43]. However, the relationship between MYC target pathways, the tumor microenvironment, and prognosis in AML remains elusive. Our findings are in line with previous reports that have demonstrated an association between the activation of the unfolded protein response and more favorable outcomes in AML [44]. The APMAO score was found to be associated with distinct variations in the immune landscape of AML, a factor that has been implicated in determining

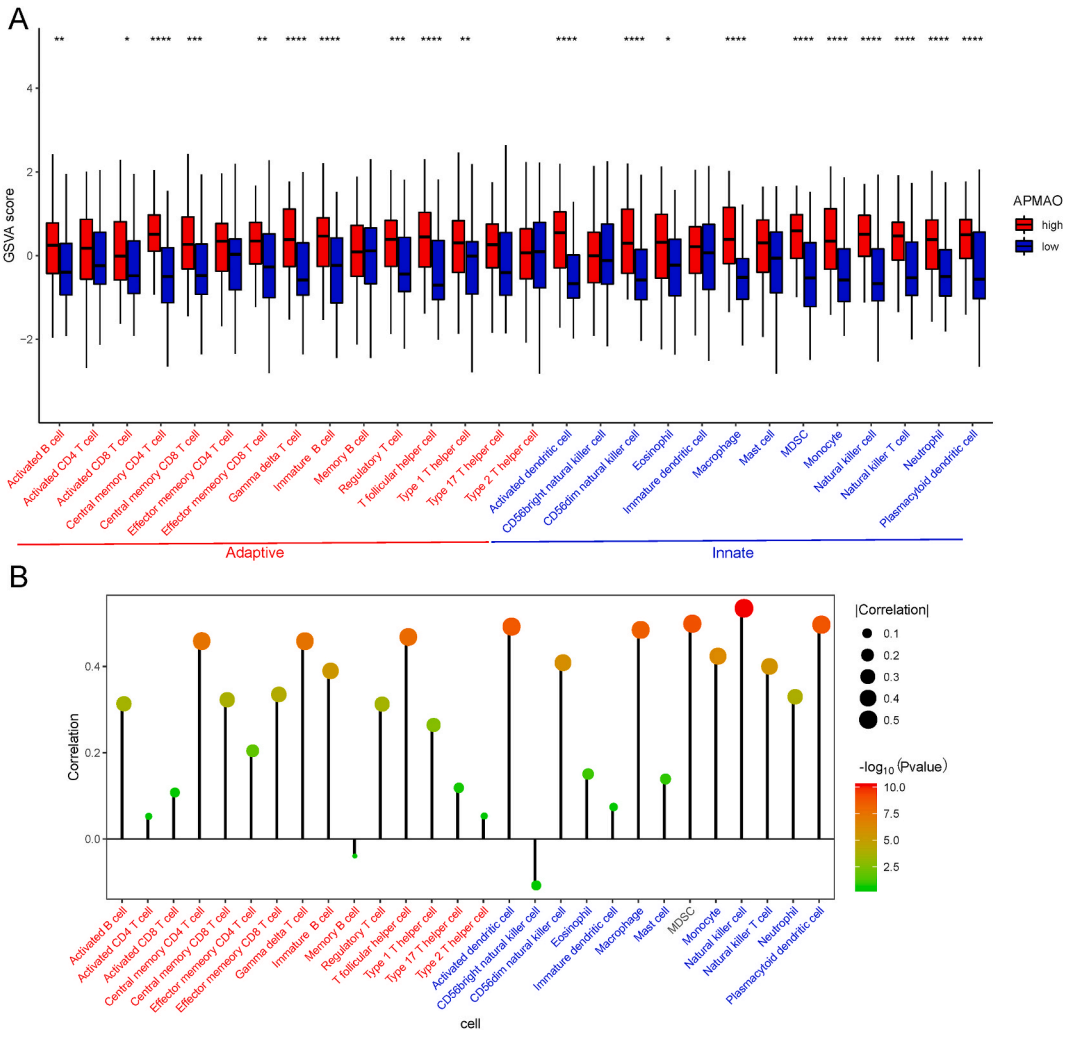

Fig. 11. Differences in tumor immune infiltration patterns stratified by APMAO (Accurate Prediction Model of AML Overall Survival) scores in acute myeloid leukemia (AML) samples. (A) Heatmap representation of the enrichment score distributions for 28 distinct immune cell populations across AML cases segregated into high and low APMAO score groups. (B) Bubble plot visualizing the correlation between continuous APMAO scores and the corresponding enrichment profiles of tumor-infiltrating immune populations.

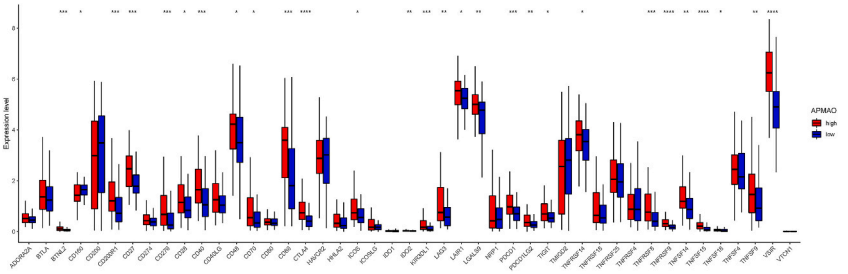

Fig. 12. Transcriptional profiles of immune checkpoint genes stratified by APMAO (Accurate Prediction Model of AML Overall Survival) scores in acute myeloid leukemia (AML). The plot depicts the expression patterns of 45 genes encoding immune checkpoint molecules across AML cases segregated into high (red) and low (blue) APMAO score groups. The x-axis lists the specific checkpoint genes, while the y-axis represents the normalized gene expression values. Each data point corresponds to the expression level of the respective gene in an individual patient sample, with the horizontal bars indicating the median expression level within each APMAO group. Statistically significant differences in expression between the high and low APMAO cohorts are denoted by asterisks above the relevant gene symbols, adhering to the following convention: ****$p < 0.0001$; ***$p < 0.001$; **$p < 0.01$; *$p < 0.05$. Genes exhibiting higher expression in the high APMAO subset are highlighted in red, while those with elevated expression in the low APMAO group are depicted in blue.

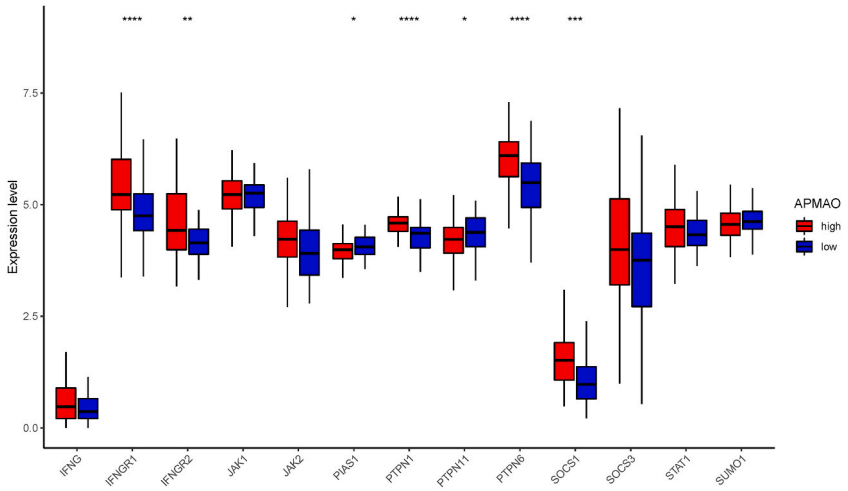

Fig. 13. Expression profiles of interferon-gamma (IFN-γ) pathway genes in acute myeloid leukemia (AML) stratified by APMAO (Accurate Prediction Model of AML Overall Survival) scores. The panel illustrates the expression levels of 13 genes involved in the IFN-γ signaling cascade across AML patient samples segregated into high (red) and low (blue) APMAO score groups. The x-axis lists the specific IFN-γ pathway genes, while the y-axis represents the normalized expression values. Statistically significant differences in expression between the high and low APMAO subgroups are highlighted by asterisks above the respective gene symbols, following the convention: ****$p < 0.0001$; ***$p < 0.001$; **$p < 0.01$; *$p < 0.05$. Genes exhibiting higher expression in the elevated APMAO subset are depicted in red, whereas those with increased expression in the low APMAO group are shown in blue.

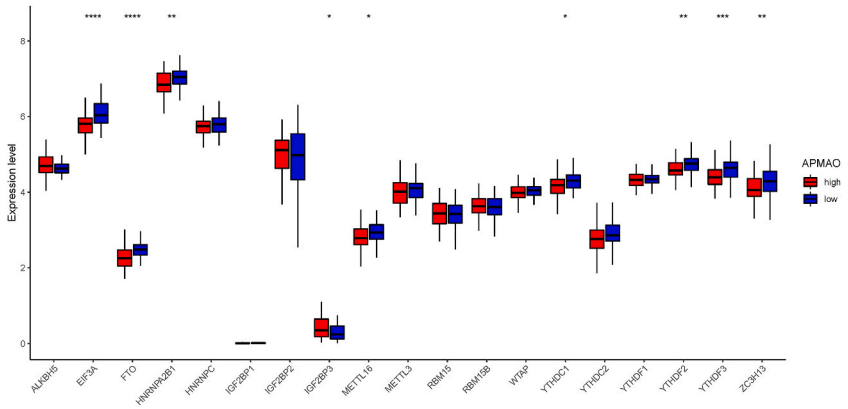

Fig. 14. Differential expression patterns of m6A regulatory genes in acute myeloid leukemia (AML) samples stratified by APMAO (Accurate Prediction Model of AML Overall Survival) scores. The panel depicts the expression levels of various genes involved in m6A methylation regulation across AML cases segregated into high and low APMAO score groups. The y-axis represents the normalized gene expression values, while the x-axis lists the specific m6A regulator genes. Statistically significant differences in expression between the high and low APMAO cohorts are denoted by asterisks, following the convention: ****$p < 0.0001$; ***$p < 0.001$; **$p < 0.01$; *$p < 0.05$.

the response to immunotherapeutic interventions [45]. Consonant with these findings, the expression patterns of immune checkpoint genes, interferon-γ pathway markers, and m6A regulators exhibited distinct signatures that were associated with the stratification of APMAO score profiles. Of note, the CD160 expression level was found negatively associated with APMAO. CD160 regulated natural killer (NK) cell cytolysis and its downregualtion has been implicated as a marker of immune escape [46] and has been patented biomarker of improved prognosis represented by its upregulation [47]. Interferon-γ signaling is involved in tumor immune responses and prolonged activation can promote chemoresistance in AML [45,48].The role of m6A methylation has garnered significant attention as a pivotal regulatory mechanism that sculpts the tumor immune microenvironment and modulates the response to immune checkpoint inhibitor therapies. Earlier studies have reported that a specific m6A methylation pattern, characterized by elevated levels of YTHDC1, is predictive of improved prognosis in AML [49].This finding aligns with our observation of higher YTHDC1 expression in the low APMAO group. However, an opposing trend was observed for ZC3H13. Taken together, these results indicate that APMAO scores exhibit a significant association with the tumor immune environment and the expression of genes related to cancer immunotherapy.

It is imperative to underscore the prospective clinical utilities of the APMAO model. This score, which amalgamates transcriptomic

data with clinical parameters, furnishes a comprehensive instrument for risk stratification and prognostic prediction in patients with AML. Through the delineation of patients into high- and low-risk cohorts, the APMAO score can inform treatment intensity and aid in the identification of individuals who may derive benefit from more aggressive or targeted therapeutic modalities.For example, high-risk patients predicted by the APMAO score may be candidates for intensive chemotherapy regimens, allogeneic stem cell transplantation, or novel targeted agents. Conversely, low-risk patients may be spared from unnecessary toxicities associated with overly aggressive treatments and could be considered for less intensive approaches or clinical trials evaluating de-escalation strategies. Furthermore, the association of the APMAO score with immunotherapy-related gene expression patterns suggests its potential utility in predicting response to emerging immunotherapeutic approaches in AML, such as checkpoint inhibitors or CAR T-cell therapy. Patients with high APMAO scores exhibiting an immunologically "hot" tumor microenvironment may be more likely to benefit from immunotherapies, while those with low scores may require alternative treatment strategies or combination approaches to overcome immunosuppressive barriers. By providing a framework for precision immunotherapy, the APMAO score represents a significant step towards realizing the promise of personalized medicine in AML.To facilitate the clinical application of the APMAO model, we plan to develop a user-friendly web-based platform that allows clinicians to easily input patient data and obtain prognostic and predictive information based on the APMAO score. This platform will provide a practical tool for clinical decision-making and will be made freely accessible to the medical community. We will also provide detailed instructions and educational materials to guide users on the appropriate interpretation and utilization of the APMAO score in various clinical scenarios.

Our study identified significant associations between the APMAO score and the expression patterns of several immunotherapy sensitivity markers, including immune checkpoint genes, interferon-γ pathway markers, and m6A regulators. These findings suggest that the APMAO score may have potential utility in stratifying AML patients for immunotherapy approaches. For instance, the higher expression of immune checkpoint genes, such as CD27, CD40, and PD-L2 (PDCD1LG2), in the high APMAO group indicates that these patients might be more likely to respond to immune checkpoint inhibitors targeting these pathways. Conversely, the lower expression of CD160 in the high APMAO group suggests that therapies targeting this checkpoint might be less effective in these patients. The differential expression of interferon-γ pathway markers between APMAO subgroups also has potential clinical implications. The higher expression of IFNGR1, IFNGR2, and SOCS1 in the high APMAO group suggests that these patients may have a more active interferon-γ signaling, which could influence their response to immunotherapies that modulate this pathway. Similarly, the distinct expression patterns of m6A regulators between APMAO subgroups raise the possibility of targeting these epigenetic modulators to enhance immunotherapy efficacy in specific patient subsets. Furthermore, the correlation between APMAO scores and immune cell infiltration patterns provides additional insights into the immunological contexture of AML tumors. The higher infiltration of certain immune cell types, such as macrophages and dendritic cells, in the high APMAO group suggests that these patients may have a more immunogenic tumor microenvironment, which could be exploited by immunotherapeutic strategies that harness these immune cells. Collectively, these findings underscore the potential of the APMAO score as a tool for patient selection and stratification in the context of AML immunotherapy. By integrating the APMAO score with immunotherapy sensitivity markers and immune cell infiltration patterns, clinicians could potentially identify AML patient subgroups that are more likely to benefit from specific immunotherapeutic approaches, enabling a more personalized treatment strategy.

The effectiveness of immunotherapy is dependent on a multitude of factors, including the composition of the tumor microenvironment, the expression levels of immune checkpoint molecules, and the activation status of cytokine signaling pathways. In this study, we observed that samples with high APMAO scores exhibited enrichment in several tumor-associated pathways, such as NFκB, TNF, JAK-STAT, and Notch signaling, which are known to play pivotal roles in modulating the immune landscape within the tumor microenvironment. Furthermore, the APMAO score exhibited a notable association with the expression patterns of immune checkpoint genes, interferon-γ pathway markers, and m6A regulatory elements. These observations intimate that the APMAO score may hold promise as a potential predictive biomarker for immunotherapeutic sensitivity, by virtue of its ability to encapsulate the intricate interplay among these critical determinants of treatment response. However, the efficacy of immunotherapy is also influenced by other factors, such as antigen presentation, T cell exhaustion, and tumor heterogeneity. Future studies need to further explore the relationship between the APMAO score and these factors and validate its ability to predict immunotherapy efficacy in clinical trials. In conclusion, the APMAO score provides a comprehensive tool for predicting prognosis and immunotherapy sensitivity in AML patients, but more research is needed to fully elucidate its mechanism of action and clinical application value in immunotherapy.

Over the past few years, the field of artificial intelligence (AI) has witnessed widespread adoption of its methodologies for prognostic modeling and therapeutic decision support in oncology. Several studies [50–54] have used machine learning and deep learning algorithms to build models for predicting prognosis and treatment response in AML. For instance, Rong et al. employed machine learning methods, including consensus clustering, Cox regression, and LASSO regression, to identify AML subtypes based on histone methylation regulators and establish the *M*-RiskScore model for predicting prognosis and chemotherapy response in AML patients [51]. The study by Zeng et al. harnessed machine learning techniques, such as clustering analysis and LASSO-Cox regression, to develop a prognostic model for acute myeloid leukemia (AML) predicated on the stratification of the tumor immune microenvironment (TIME). The model's predictive performance was assessed using receiver operating characteristic (ROC) curves and the concordance index (*C*-index) [52]. Shreve et al. constructed a personalized risk stratification model for AML patients by harnessing the power of the XGBOOST machine learning algorithm, which integrates clinical, cytogenetic, and mutational data. This innovative approach demonstrated superior performance compared to the widely used European LeukemiaNet (ELN) classification system, highlighting its potential to revolutionize risk assessment in AML [53]. Furthermore, cutting-edge deep learning architectures, including convolutional neural networks (CNNs) and recurrent neural networks (RNNs), have been leveraged to advance the understanding and modeling of acute myeloid leukemia (AML). Matek et al. curated an extensive annotated image dataset of white blood cells and utilized it to train a CNN model capable of classifying leukocytes and identifying blast cells in AML with a level of accuracy comparable to human experts.

This groundbreaking work highlights the immense potential of deep learning techniques in facilitating the early detection of malignant cell populations in AML, paving the way for improved diagnostic and prognostic strategies [54]. Ramya et al. introduced a novel hybrid deep learning framework that integrates a Convolutional Neural Network (CNN), Bidirectional Long Short-Term Memory (Bi-LSTM), and Recurrent Neural Network (RNN) architectures, which are optimized using the innovative Slime Mould Algorithm. This sophisticated approach aims to achieve accurate detection of Acute Myeloid Leukemia (AML) from morphological images by sequentially employing preprocessing, segmentation, feature extraction, and classification techniques. The proposed model showcases the immense potential of synergistic deep learning methodologies in enhancing the efficiency and reliability of AML diagnosis based on visual data [50]. Our APMAO score model integrates gene expression and clinical data using machine learning methods such as multivariate Cox regression and LASSO regression to build a comprehensive prognostic tool for AML. Compared to existing studies, our model not only considers transcriptomic features but also incorporates key clinical factors such as cytogenetics and FAB classification, providing a more comprehensive and accurate prognostic prediction. Furthermore, we explored the association between the APMAO score and immunotherapy-related markers, offering new insights into personalized immunotherapy for AML. Taken together, our research complements previous work and collectively advances the application of AI in precision medicine for AML.

Our study has several limitations that should be considered. Firstly, unmeasured confounding variables, like patient performance status, comorbidities, and treatment regimens, could influence the accuracy of our prognostic model. Incorporating these factors in future studies is essential. Secondly, our study relied solely on transcriptomic data, and integrating multi-omics data could provide deeper insights into the molecular mechanisms of AML prognosis. While we identified associations between the APMAO score and immune-related factors, these findings require experimental validation through functional studies and clinical trials. The generalizability of our results may be limited due to the heterogeneity of AML and the relatively small sample size. Our study included cytogenetic risk stratification but did not consider more granular molecular subtypes. Validation in larger, prospective cohorts encompassing diverse AML subtypes is necessary. Additionally, our study is based on retrospective data analysis, which has inherent limitations in data quality, completeness, and potential selection biases. Prospective validation of the APMAO score in well-designed clinical studies is crucial to establish its utility and robustness in real-world settings. It should be noted that another limitation of this study is the lack of detailed treatment information in the TCGA database, which only records whether therapy was administered but not the specific drugs and dosages used. This may introduce bias and affect the accuracy of our model in predicting chemotherapy drug efficacy. Future studies should aim to incorporate more comprehensive treatment data, including specific therapeutic agents and dosing schedules, to enable more precise modeling of treatment response. Collaborative efforts to pool detailed clinical data from multiple institutions and clinical trials may help address this limitation and improve the predictive power of prognostic models like APMAO. Despite these limitations, our study provides a valuable framework for integrating molecular and clinical data to develop a prognostic model for AML. The limitations highlighted here offer important opportunities for future research to refine and extend our findings.

In summary, the current study demonstrated the robust prognostic value of the developed APMAO scoring system in acute myeloid leukemia (AML), consistently correlating with distinct patterns across clinicopathological, mutational, functional, immune cell landscape, and cancer immunotherapy-related gene expression profiles. However, the lack of experimental validation in an independent clinical cohort and the inherent batch effects associated with multi-cohort analyses pose limitations to the findings. The results presented herein should serve as a foundation for further research aimed at validating the utility of the APMAO scoring system, particularly in diverse clinical and molecular subgroups of AML, to establish its potential for widespread application in clinical practice.

Ethics approval and consent to participate

Not applicable.

Availability of data and materials

GSE37642 (weblink [39]), GSE12417 (weblink: https://www.ncbi.nlm.nih.gov/geo/query/acc.cgi?acc=GSE12417), GSE10358 (weblink: https://www.ncbi.nlm.nih.gov/geo/query/acc.cgi?acc=GSE10358), GSE146173 (URL: https://www.ncbi.nlm.nih.gov/geo/query/acc.cgi?acc=GSE146173), and GSE106291 (URL: https://www.ncbi.nlm.nih.gov/geo/query/acc.cgi?acc=GSE106291) dataset were obtained from the Gene Expression Omnibus (GEO) database (URL: https://www.ncbi.nlm.nih.gov/geo/), while the TCGA-LAML data was acquired from The Cancer Genome Atlas (TCGA) database (https://portal.gdc.cancer.gov/). All the data generated or analyzed during the course of this study have been included in this published article and its accompanying supplementary information files.

Funding statement

This research was supported by grants from the Science and Technology Program of the Jiangxi Provincial Administration of Traditional Chinese Medicine (grant numbers 2022B967 and 2021B363) and the Science and Technology Plan Project of the Jiangxi Provincial Health Care Commission (grant number 202212543).

CRediT authorship contribution statement

Yiyun Pan: Writing – original draft, Data curation. **Wen Zeng:** Writing – review & editing, Funding acquisition, Formal analysis. **Xiaoming Nie:** Validation, Methodology. **Hailong Chen:** Visualization, Supervision. **Chuanhua Xie:** Methodology, Investigation. **Shouju Guo:** Supervision, Project administration. **Dechang Xu:** Writing – review & editing, Supervision, Resources. **Yijian Chen:** Writing – review & editing, Validation, Funding acquisition, Conceptualization.

Declaration of generative AI and AI-assisted technologies in the writing process

In the process of preparing this manuscript, the authors employed the language model ChatGPT to assist in refining the linguistic presentation of the work. Following the use of this tool, the authors meticulously reviewed and revised the content as necessary, and they assume full responsibility for the entirety of the published material.

Declaration of competing interest

The authors declare that they have no known competing financial interests or personal relationships that could have appeared to influence the work reported in this paper.

Acknowledgements

Not applicable.

Appendix ASupplementary data

Supplementary data to this article can be found online at https://doi.org/10.1016/j.heliyon.2024.e32154.

References

[1] Epidemiology of acute myeloid leukemia: Recent progress and enduring challenges , Blood, Rev 36 (2019 Jul) 70–87.
[2] F. Ferrara, C.A. Schiffer, Acute myeloid leukaemia in adults, Lancet 381 (9865) (2013) 484–495.
[3] R.L. Siegel, K.D. Miller, A. Jemal, Cancer statistics, 2019, CA A Cancer J. Clin. 69 (1) (2019 Jan) 7–34.
[4] M. Yi, A. Li, L. Zhou, Q. Chu, Y. Song, K. Wu, The global burden and attributable risk factor analysis of acute myeloid leukemia in 195 countries and territories from 1990 to 2017: estimates based on the global burden of disease study 2017, J. Hematol. Oncol. 13 (1) (2020 Dec) 72.
[5] The Cancer Genome Atlas Research Network, Genomic and epigenomic landscapes of adult de novo acute myeloid leukemia, N. Engl. J. Med. 368 (22) (2013 May 30) 2059–2074.
[6] H. Döhner, E. Estey, D. Grimwade, S. Amadori, F.R. Appelbaum, T. Büchner, et al., Diagnosis and management of AML in adults: 2017 ELN recommendations from an international expert panel, Blood J. Am. Soc. Hematol. 129 (4) (2017) 424–447.
[7] D.A. Arber, A. Orazi, R. Hasserjian, J. Thiele, M.J. Borowitz, M.M. Le Beau, et al., The 2016 revision to the World Health Organization classification of myeloid neoplasms and acute leukemia, Blood J. Am. Soc. Hematol. 127 (20) (2016) 2391–2405.
[8] M. Arnone, M. Konantz, P. Hanns, A.M. Paczulla Stanger, S. Bertels, P.S. Godavarthy, et al., Acute myeloid leukemia stem cells: the challenges of phenotypic heterogeneity, Cancers 12 (12) (2020) 3742.
[9] W. Zeijlemaker, J.W. Gratama, G.J. Schuurhuis, Tumor heterogeneity makes AML a "moving target" for detection of residual disease: phenotype instability and MRD in AML, Cytometry B Clin. Cytom. 86 (1) (2014) 3–14.
[10] H. Döhner, A.H. Wei, B. Löwenberg, Towards precision medicine for AML, Nat. Rev. Clin. Oncol. 18 (9) (2021) 577–590.
[11] W. Hofmann, A. Trumpp, C. Müller-Tidow, Therapy resistance mechanisms in hematological malignancies, Int. J. Cancer 152 (3) (2023 Feb) 340–347.
[12] C.R. Wiggers, M.L. Baak, E. Sonneveld, E.E. Nieuwenhuis, M. Bartels, M.P. Creyghton, AML subtype is a major determinant of the association between prognostic gene expression signatures and their clinical significance, Cell Rep. 28 (11) (2019) 2866–2877.
[13] W.Y. Cheng, J.F. Li, Y.M. Zhu, X.J. Lin, L.J. Wen, F. Zhang, et al., Transcriptome-based molecular subtypes and differentiation hierarchies improve the classification framework of acute myeloid leukemia, Proc. Natl. Acad. Sci. USA 119 (49) (2022 Dec 6) e2211429119.
[14] S. Stratmann, S.A. Yones, M. Garbulowski, J. Sun, A. Skaftason, M. Mayrhofer, et al., Transcriptomic analysis reveals proinflammatory signatures associated with acute myeloid leukemia progression, Blood Adv. 6 (1) (2022) 152–164.
[15] Y. Lai, L. Sheng, J. Wang, M. Zhou, G. OuYang, A novel 85-gene expression signature predicts unfavorable prognosis in acute myeloid leukemia, Technol. Cancer Res. Treat. 20 (2021 Jan 1), 153303382110049.
[16] B. Lai, Y. Lai, Y. Zhang, M. Zhou, G. OuYang, Survival prediction in acute myeloid leukemia using gene expression profiling, BMC Med. Inf. Decis. Making 22 (1) (2022 Dec) 57.
[17] D.R. Silveira, L. Quek, I.S. Santos, A. Corby, J.L. Coelho-Silva, D.A. Pereira-Martins, et al., Integrating clinical features with genetic factors enhances survival prediction for adults with acute myeloid leukemia, Blood Adv. 4 (10) (2020) 2339–2350.
[18] F. Damm, M. Heuser, M. Morgan, K. Wagner, K. Görlich, A. Großhennig, et al., Integrative prognostic risk score in acute myeloid leukemia with normal karyotype, Blood J. Am. Soc. Hematol. 117 (17) (2011) 4561–4568.
[19] A. Walker, G. Marcucci, Molecular prognostic factors in cytogenetically normal acute myeloid leukemia, Expert Rev. Hematol. 5 (5) (2012 Oct) 547–558.
[20] Y. Tazi, J.E. Arango-Ossa, Y. Zhou, E. Bernard, I. Thomas, A. Gilkes, et al., Unified classification and risk-stratification in acute myeloid leukemia, Nat. Commun. 13 (1) (2022) 1–16.
[21] IL-8 as mediator in the microenvironment-leukaemia network in acute myeloid leukaemia - PubMed [Internet]. [cited 2024 Mar 13]. Available from: https://pubmed.ncbi.nlm.nih.gov/26674118/.
[22] Isolated trisomy 13 defines a homogeneous AML subgroup with high frequency of mutations in spliceosome genes and poor prognosis, Blood 124 (8) (2014 Aug 21) 1304–1311.
[23] A 29-gene and cytogenetic score for the prediction of resistance to induction treatment in acute myeloid leukemia, Haematologica 103 (3) (2018 Mar) 456–465.

[24] Identification of a 24-gene prognostic signature that improves the European LeukemiaNet risk classification of acute myeloid leukemia: an international collaborative study, J Clin Oncol 31 (9) (2013 Mar 20) 1172–1181.
[25] Ensembl 2022, Nucleic Acids Res. 50 (2022) D988–D995. D1.
[26] P. Charoentong, F. Finotello, M. Angelova, C. Mayer, M. Efremova, D. Rieder, et al., Pan-cancer immunogenomic analyses reveal genotype-immunophenotype relationships and predictors of response to checkpoint blockade, Cell Rep. 18 (1) (2017 Jan 3) 248–262.
[27] J.G. Tate, S. Bamford, H.C. Jubb, Z. Sondka, D.M. Beare, N. Bindal, et al., COSMIC: the catalogue of somatic mutations in cancer, Nucleic Acids Res. 47 (D1) (2019 Jan 8) D941–D947.
[28] Signatures of T, cell dysfunction and exclusion predict cancer immunotherapy response, Nat Med 24 (10) (2018 Oct) 1550–1558.
[29] Apollo, An accurate and independently validated prediction model of lower-grade gliomas overall survival and a comparative study of model performance, EBiomedicine 79 (2022 May) 104007..
[30] C. Baldazzi, S. Luatti, G. Marzocchi, A. Grassi, M. Cavo, N. Testoni, t(5;12)(q31;p13)/ETV6::ACSL6 and t(6;9)(p23;q34)/DEK::NUP214 concurrence in acute myeloid leukemia: an unusual association of two rare abnormalities, Cancer Genet 262–263 (2022 Apr) 35–39.
[31] M. Milella, S.M. Kornblau, Z. Estrov, B.Z. Carter, H. Lapillonne, D. Harris, et al., Therapeutic targeting of the MEK/MAPK signal transduction module in acute myeloid leukemia, J. Clin. Invest. 108 (6) (2001 Sep) 851–859.
[32] Acute myeloid leukemia with t(4;12)(q12;p13): report of 2 cases, Blood Res 23 (2016 Jun).
[33] A. Koleilat, P.W. McGarrah, H. Olteanu, D.L. Van Dyke, J.B. Smadbeck, S.H. Johnson, et al., Utilizing next-generation sequencing to characterize a case of acute myeloid leukemia with t(4;12)(q12;p13) in the absence of ETV6/CHIC2 and ETV6/PDGFRA gene fusions, Cancer Genet 260–261 (2022 Jan) 1–5.
[34] J. Wang, M. Yu, Q. Guo, Q. Ma, C. Hu, Z. Ma, et al., Prognostic significance of huntingtin interacting protein 1 expression on patients with acute myeloid leukemia, Sci. Rep. 7 (2017 Apr 28) 45960.
[35] A.V. Mena-Duran, J.C. Pajuelo, J. Cervera-Zamora, Z. Garcia-Casado, A. Valencia, E. Barragan, et al., SHP-1 (PTPN6) Gene Supression by FLT3/ITD Defines an Aggressive Subgroup of Myeloid Malignancies [Internet], American Society of Hematology, 2006 [cited 2024 Mar 13]. Available from: https://ashpublications.org/blood/article-abstract/108/11/1907/127832.
[36] A. Beghini, C.B. Ripamonti, P. Peterlongo, G. Roversi, R. Cairoli, E. Morra, et al., RNA hyperediting and alternative splicing of hematopoietic cell phosphatase (PTPN6) gene in acute myeloid leukemia, Hum. Mol. Genet. 9 (15) (2000 Sep 22) 2297–2304.
[37] Y. Ben-Neriah, A. Venkatachalam, A. Fink, E. Hung, J. Vacca, F. Mercurio, et al., Targeting the transcriptional addiction of leukemia stem cells by a new class of protein kinase inhibitors, Blood 130 (2017) 812.
[38] E. Lalli, J. Alonso, Targeting DAX-1 in embryonic stem cells and cancer, Expert Opin. Ther. Targets 14 (2) (2010 Feb) 169–177.
[39] Z. Chen, J. Song, W. Wang, J. Bai, Y. Zhang, J. Shi, et al., A novel 4-mRNA signature predicts the overall survival in acute myeloid leukemia, Am. J. Hematol. 96 (11) (2021 Nov 1) 1385–1395.
[40] European LeukemiaNet 2017 risk stratification for acute myeloid leukemia: validation in a risk-adapted protocol, Blood Adv. 6 (4) (2022 Feb 22) 1193–1206.
[41] T.J. Ley, L. Ding, M.J. Walter, M.D. McLellan, T. Lamprecht, D.E. Larson, et al., DNMT3A mutations in acute myeloid leukemia, N. Engl. J. Med. 363 (25) (2010 Dec 16) 2424–2433.
[42] Q. Jia, J. Wang, N. He, J. He, B. Zhu, Titin mutation associated with responsiveness to checkpoint blockades in solid tumors, JCI Insight 4 (10) (2019 May 16) e127901, 127901.
[43] MYC protein expression is an important prognostic factor in acute myeloid leukemia, Leuk Lymphoma 60 (1) (2019 Jan) 37–48.
[44] Activation of the unfolded protein response is associated with favorable prognosis in acute myeloid leukemia, Clin Cancer Res. 15 (11) (2009 Jun 1) 3834–3841.
[45] Immune landscapes predict chemotherapy resistance and immunotherapy response in acute myeloid leukemia, Sci Transl Med. 12 (546) (2020 Jun 3) eaaz0463.
[46] Z.H. Wang, H.H. Liu, N. Ma, L.H. Wang, W. Liu, B. Tang, et al., [A preliminary study on the expression of CD160 on NK cells and its mechanism of mediating NK killing effect], Zhongguo Shi Yan Xue Ye Xue Za Zhi 26 (5) (2018 Oct) 1559–1564.
[47] E. Vivier, E. Narni-Mancinelli, B. Escaliere, P.Y. Dumas, A. Crinier, Use of Cd160 as a Biomarker in Acute Myeloid Leukemia [Internet], Google Patents, 2022 [cited 2024 Mar 13]. Available from: https://patents.google.com/patent/WO2022013256A1/en.
[48] J. Vadakekolathu, S. Reeder, C. Coveney, S. Rutella, Tipifarnib modulates interferon (IFN)-γ-Inducible genes in acute myeloid leukemia, Blood 134 (2019) 2726.
[49] S. Han, J. Qi, K. Fang, H. Wang, Y. Tang, D. Wu, et al., Characterization of m6A regulator-mediated methylation modification patterns and tumor microenvironment infiltration in acute myeloid leukemia, Cancer Med. 11 (5) (2022 Mar) 1413–1426.
[50] V.J. Ramya, S. Lakshmi, An efficient hybrid model for acute myeloid leukaemia detection using convolutional Bi-lstm based recurrent neural network, Comput Methods Biomech Biomed Eng Imaging Vis 11 (3) (2023 May 4) 413–424.
[51] D. Rong, X. Chen, J. Xiao, D. Liu, X. Ni, X. Tong, et al., Histone methylation modification patterns and relevant M-RiskScore in acute myeloid leukemia, Heliyon 8 (9) (2022 Sep) e10610.
[52] T. Zeng, L. Cui, W. Huang, Y. Liu, C. Si, T. Qian, et al., The establishment of a prognostic scoring model based on the new tumor immune microenvironment classification in acute myeloid leukemia, BMC Med. 19 (1) (2021 Aug 5) 176.
[53] J. Shreve, M. Meggendorfer, H. Awada, S. Mukherjee, W. Walter, S. Hutter, et al., A personalized prediction model to risk stratify patients with acute myeloid leukemia (AML) using artificial intelligence, Blood 134 (2019 Nov 13), 2091.
[54] C. Matek, S. Schwarz, K. Spiekermann, C. Marr, Human-level recognition of blast cells in acute myeloid leukaemia with convolutional neural networks, Nat. Mach. Intell. 1 (11) (2019 Nov) 538–544.